NASA Technical Memorandum 108860

Flow Visualization Studies of VTOL Aircraft Models During Hover In Ground Effect

Nikos J. Mourtos, Stephane Couillaud, and Dale Carter, San Jose State University, San Jose, California
Craig Hange, Doug Wardwell, and Richard J. Margason, Ames Research Center, Moffett Field, California

January 1995

National Aeronautics and Space Administration

Ames Research Center
Moffett Field, California 94035-1000

Flow Visualization Studies of VTOL Aircraft Models During Hover In Ground Effect

NIKOS J. MOURTOS,* STEPHANE COUILLAUD,* DALE CARTER,* CRAIG HANGE,
DOUG WARDWELL, AND RICHARD J. MARGASON

Ames Research Center

Summary

A flow visualization study of several configurations of a jet-powered vertical takeoff and landing (VTOL) model during hover in ground effect was conducted. A surface oil flow technique was used to observe the flow patterns on the lower surfaces of the model. Wing height with respect to fuselage and nozzle pressure ratio are seen to have a strong effect on the wing trailing edge flow angles. This test was part of a program to improve the methods for predicting the hot gas ingestion (HGI) for jet-powered vertical/short takeoff and landing (V/STOL) aircraft. The tests were performed at the Jet Calibration and Hover Test (JCAHT) Facility at Ames Research Center.

Introduction

Jet-powered vertical/short takeoff and landing (V/STOL) airplanes can experience significant performance losses during hover and during transition between hover and wing-borne flight. These losses are caused by the propulsion efflux. Two propulsion-induced effects are especially critical during operation near the ground for takeoff or landing: (1) jet-induced effects on aerodynamics and (2) hot gas ingestion (HGI) effects on engine performance.

HGI is a term used to describe any flow mechanism where hot exhaust gas from a propulsion jet returns to the inlet of the same propulsion system. Three flow patterns that cause HGI in jet-powered V/STOL aircraft are shown in figure 1. Figure 1(a) shows the flow field for a multiple-jet configuration in ground effect. The hot jets impinge on the ground and form wall jets which may run into each other underneath the airplane and form a fountain. This fountain brings the hot exhaust gases very rapidly to the airplane's undersurface where they impinge forming a lateral stagnation line in the spanwise direction. At the side of the fuselage or at the edge of the wing planform some of the flow continues upward where it may find its way into the engine inlets. Between this stagnation line and both the front and rear jets, the fountain fluid flows along the fuselage lower surface toward the jets where it is entrained by the jet and forms a vortex pair as sketched in figure 1(a). The jet efflux and the fountain flow entrain ambient temperature air which produces a nonuniform temperature profile. This recirculation is called near-field HGI and can cause a rapid increase in the inlet temperature which in turn decreases the thrust. In addition, uneven temperature distribution can result in inlet flow distortion and cause compressor stall. In addition, the fountain-induced vortex pair can cause a lift loss and a pitching-moment increment.

Figures 1(b) and 1(c) show the flow field for a single-jet configuration. The effects of wind (fig. 1(b)) and buoyancy (fig. 1(c)) bring the hot gases back into the engine inlets. This recirculation is called far-field HGI. Multiple-jet configurations may also experience far-field HGI. As illustrated in figure 1(b), far-field HGI can occur rapidly when there is a crosswind blowing the hot exhaust back to the inlet or when the aircraft speed causes a similar relative motion between the hot gases and the engine inlet. Depending on the wind speed, aircraft speed, and aircraft geometry, there is a wind speed which produces a maximum temperature rise. At either greater or lesser speeds the temperature rise is reduced because the hot gases from the far field are convected away from the engine inlets. However, buoyancy effects (fig. 1(c)) take time to become established. For the AV-8 Harrier, it takes about 30 seconds in hover for the air around it to heat up by 5°C. This 5°C increase in air temperature entering the inlet reduces the thrust by about 4 percent.

Near-field HGI tends to bring hot exhaust gases quickly into the engine inlets. For the AV-8 Harrier, in about one second during hover the fountain effect can increase the inlet temperature by as much as 10°C. This temperature increase results in approximately 10 percent loss of thrust, which is significant considering the fact that the thrust-to-weight ratio for most V/STOL airplanes is only 10 to 30 percent greater than one. The Harrier, however, does not represent the worse case scenario for HGI. In some jet VTOL airplane models an inlet temperature rise (ITR) of 55°C has been measured (refs. 1 and 2) after only a very

*San Jose State University, San Jose, California.

short time in hover within ground effect. Such values of ITR can cause a major loss of thrust and consequently a crash.

The HGI problem was recognized (ref. 3) and considered during the research and development of the Harrier in the late 1950s. In the mid 1960s, NASA initiated several experimental projects (refs. 1, 2, 4–7) to obtain HGI data. Additional research was done in Europe (refs. 8–10), especially for the VAK-191B VTOL aircraft. The recent U.S./U.K. advanced short takeoff and vertical landing (ASTOVL) aircraft studies have generated a renewed interest in the topic as shown by current experimental investigations (ref. 11) of some of the basic mechanisms and configuration effects.

In the late 1960s and early 1970s, the first attempts were made to develop analytical methods for HGI. An early empirical approach by Behnert (ref. 9) was developed in support of the VAK-191B VTOL aircraft program. This method was based on a correlation of the small-scale model data and the full-scale aircraft data. In 1971, Gray and Kisielowski (ref. 12) developed an engineering method for predicting the temperatures and velocities in the vicinity of vertical lift engines of jet V/STOL aircraft operating near the ground. This method described the propulsion efflux flow field starting at the lift jet exit, continuing to ground impingement through the wall jet to either a far-field flow or to a fountain flow back up to the aircraft and the engine inlets. The effects of both near-field and wind-generated far-field recirculation were included. Barron and Frauenberger (ref. 13) applied this analysis in an early code that evaluated jet-induced ground footprint and hot gas upwash characteristics of V/STOL aircraft.

In the early 1980s, Green and Zanine (refs. 14–16) extended and implemented the methods of reference 12 in a computer program, REINGST, to attempt a rapid, preliminary design estimation of inlet temperature rise due to near- and far-field HGI for a jet VTOL aircraft. The method was compared by its authors with the limited experimental data which were available at the time and found to achieve reasonable success for several aircraft. Currently, this is the only nonproprietary code that is available for estimating HGI. The REINGST code was reevaluated in 1990 (ref. 17) to establish its effectiveness for several V/STOL aircraft configurations. Unfortunately, the method greatly underpredicted the ITR due to near-field recirculation because of inaccurate empirical correlations for the temperature decay in the various regions of the flow field. In addition, the method failed to account properly for the geometry of the airplane. This HGI prediction method (refs. 14–16) assumes that the aircraft has a flat undersurface; as shown in reference 17, the agreement with experimental data which involved three-dimensional (3-D) models was not very good. This result demonstrated the need to study flow fields around 3-D models to obtain a better understanding of the mechanisms which cause HGI.

The purpose of the present flow visualization investigation was to use a simple two-jet geometry to evaluate the effect of model configuration (flat-plate or 3-D model), NPR, and model height on the general flow patterns which cause HGI. The flat-plate model was designed to be tested either as a body alone or as a wing-body configuration. The 3-D model was designed so that three different airplane configurations could be tested with minimum hardware changes (body alone, body with high wing, and body with low wing). The flow patterns on the lower model surface were observed using a fluorescent oil flow technique. This report presents the results of that flow visualization study.

Symbols and Acronyms

ASME	American Society of Mechanical Engineers
D_e	equivalent nozzle diameter based on the total area of all exhaust nozzles, in.
H	distance from nozzle exit to ground impingement point, in.
HGI	hot gas ingestion
HTR	hover test rig
ITR	inlet temperature rise
JCAHT	Jet Calibration and Hover Test Facility
NPR	nozzle pressure ratio
PSCL	Propulsion Simulator Calibration Laboratory
SAE	Society of Automotive Engineers
V/STOL	vertical/short takeoff and landing
VTOL	vertical takeoff and landing

Description of the Test Setup

The description of the Jet Calibration and Hover Test Facility (JCAHT) test setup includes relatively complete discussions of the hover test rig (HTR), model nozzle and plenum details, model hardware, flow visualization technique, and data acquisition system. A few features of the JCAHT which were not used in this phase of this investigation are identified in the following discussion.

However, information on the entire JCAHT is included to provide an understanding of the complete experimental facility.

Hover Test Rig

The Ames JCAHT facility (shown in fig. 2) was an extension of the Propulsion Simulator Calibration Laboratory (PSCL). JCHAT added the HTR (fig. 3), high-pressure air heaters, and jet calibration rig to the laboratory. Whereas the HTR was used in the present investigation only for flow visualization, it did use the same plenum nozzle assembly and balance mounting hardware used for metric models. In other investigations the HTR was used to measure jet-induced forces and ITR due to HGI on V/STOL models hovering in or out of ground effect.

Mounted at the top of the HTR is a six-component internal strain gage balance. As shown in figure 3(a), the model is attached perpendicular to the axial force direction of the balance. Also at the top of the rig is the plenum assembly for piping high pressure air to the jet nozzles. The entire plenum and nozzle assembly is mounted so that it does not make contact with the model suspended from the balance. This is done so that the jet-induced forces on the model are the only forces measured by the balance. Nozzle thrust is generally obtained as a function of NPR from the calibrations on the jet calibration rig. For HGI tests the model may also be instrumented with thermocouples for temperature measurements.

Underneath the model is an 8 ft × 8 ft aluminum ground board. This is lifted by a hydraulic system capable of varying height with a 1/32 in. accuracy. Instead of having the airplane model move, the ground is moved to vary model height. A string potentiometer provides the table height to the data system. A trap door is also incorporated into the ground board. Normally, for HGI testing, this door is left open while the test parameters are set to scavenge the hot simulated exhaust gases out of the room. At a data time zero, the door is quickly closed; the airplane is suddenly exposed to ground effect and near-field flow starts to form. However, for the flow visualization tests only cold air was used and the trap door was replaced by a transparent plastic sheet (fig. 3(b)). A camera mounted under the plastic was used to photograph the lower surface of the models. For a given data point, the ground plane height was adjusted to the desired value, then the nozzles were turned on to the desired NPR. After the flow stabilized, a photograph was taken.

Details of Nozzle and Plenum

The two ASME nozzles were bolted to the rectangular plenums as shown in figure 4(a). The nozzles had three internal porous plates to improve flow quality. The porous plate locations, porosities, and hole diameters are shown in figure 4(a). Details of the nozzle exit are shown in figure 4(b). The nozzle exit diameter was 1.23 in. A gap of 0.05 in. was maintained between the model and the nozzle. A fouling circuit warned of fouling between the nozzle and the model due either to physical contact or to the buildup of ice on the nozzle due to cold flow tests. For the present investigation this was not an issue because force data were not recorded.

A Kiel probe assembly (fig. 5) was used to sense the total pressure and total temperature. The Kiel probe had a shield diameter of 0.095 in. At the location of the Kiel probe (fig. 4), the inner diameter of the duct leading to the nozzle was 1.935 in. The Kiel probe was mounted in each nozzle 3.5 in. from the exit of the nozzle and 2.0 in. downstream of the last porous plate which has 0.078 in. diameter holes. As a result the 2.0 in. distance was 26 hole diameters from the downstream porous plate. This was considered to be sufficient distance to avoid any adverse influence of the porous plates on measurement accuracy.

Model Hardware

Five model configurations were tested: two were flat-plate models and three were 3-D models. Figure 6(a) shows the flat-plate body alone and figure 6(b) shows the flat-plate wing/body combination. These configurations were selected because they were similar to some which had been tested for HGI and suckdown in a previous investigation (ref. 18).

Figure 7 shows the 3-D models which were designed for this investigation. The fuselage had a simple circular cross section with an ogive nose and a blunt aft end. The model was designed to permit the wing to be mounted in either a low or high position relative to the fuselage. The wing for all model configurations was made from a flat plate and had a sharp edge as shown in figure 4(b). There were two simple circular flared inlets which could be mounted in one of the three longitudinal positions. A fairing mounted on the fuselage represented a pylon mount for the inlet ducts. Aft of the model, the ducts from each inlet were joined into a single duct on the line of symmetry. Although not used in the present investigation, this single duct could be connected to a suction source to induce flow into the simulated engine inlets.

Flow Visualization Technique

A surface oil flow technique (ref. 19) was used to visualize the flow streamlines on the undersurface of the models. Red, yellow, and blue fluorescent paint pigments were mixed with common gear oil (SAE 90 or 120). The viscosity of the mixture had to be sufficiently high so that it would not drip off or run down the surface of the model before the test began but at the same time be sufficiently low so that it would run in the direction of the boundary layer streamlines once exposed to the flow induced by the fountain upwash. Dots of these paint/oil mixtures were applied on the model undersurface in lateral rows of alternating colors for each test. The model was then mounted for testing. The fluorescent properties of the oil/pigment mixture were made visible by use of ultra-violet lamps. The flow was allowed approximately two minutes to establish itself at each height or NPR before a photograph was taken.

Data Acquisition System

The data acquisition system was used in the present investigation to monitor the model operating conditions. All of the voltage potential measurement signals from the pressure transducers and potentiometers were amplified and read into a desktop computer system outfitted with 12 bit A/D acquisition boards. The system had the ability to measure 64 independent channels at a rate close to 100,000 total samples per second per channel. A graphical user interface program was used to control the data acquisition.

Results

The test was conducted to qualitatively illustrate the effects of three important parameters on the surface flow of jet-powered V/STOL airplanes while hovering in ground effect. These parameters are the configuration of the airplane, the nozzle pressure ratio (NPR), and the height from the ground.

Five airplane model configurations were tested for a range of NPR and heights: (1) flat-plate body alone, (2) flat-plate wing/body combination, (3) round body alone, (4) round body/low flat-plate wing combination, and (5) round body/high flat-plate wing combination. The last configuration was also tested with side inlets. The fairings between the body and the inlets were left in place even when the inlets were not installed to get a more realistic representation of the fuselage flow field.

NPR values of 1.5, 3.0, 4.5, and 6.0 were tested. The height of the nozzles from the ground was varied from 3.48 to 52.2 in. or, in terms of the nozzle height to nozzle effective diameter ratio (H/D_e), values of 2, 4, 6, 8, 10, 15, 20, and 30. Above six diameters there was very little movement of the paint dots. As a consequence these photographs are not presented.

The process of applying paint to the model prior to each run was rather time consuming. Therefore, initial tests were conducted to determine the most efficient test procedure so that the available test time could be used effectively. It was found that a reduction of height usually caused a small change from the flow pattern observed at the previous height. The new flow pattern was found to agree reasonably well with that obtained at the reduced height using a new application of paint dots. As a result, the following test procedure was adopted. The oil dots were applied once in the beginning of a test run where the NPR was held constant. The model was placed at the greatest nozzle height from the ground ($H/D_e = 30$). The flow was then allowed to stabilize for three minutes before photographs were taken. Then the nozzle height was reduced to the next lower height and the above process was repeated. Thus, while the flow pattern seen at each height is accumulative from all the test points taken before it, check runs indicated that there was no adverse effect on the resultant flow patterns.

Flat-Plate Body Alone

Figure 8 shows the undersurface flow pattern for the flat-plate body alone for an NPR of 3.0 and a nozzle height of 3.48 in. ($H/D_e = 2$). The condition was selected as typical of the flow pattern which occurred at the lowest heights. The lateral fountain impingement line can be seen at the midpoint between the nozzles. The major surface flow pattern is observed to flow from the fountain impingement line toward the nozzles. Local entrainment into the jet efflux can also be seen near the nozzles.

Information about the local flow velocities can be determined from the length of any given paint dot flow pattern. To either side of the fountain region it is evident that the drops moved very quickly, because of the long length that the droplet formed in the given time. On the front side of the front nozzle, and rear side of the rear nozzle, it can be seen that the flow was very slow, and some of the droplets had not moved at all.

The red droplets in the center of the fountain region demonstrate another interesting phenomenon. Individual droplets flowed both forward and backward from where they were initially applied. This pattern was seen at the first height ($H/D_e = 6$) where the flow caused the dots to move and become more pronounced as the height was reduced further. So, most likely, the fountain actually split the droplets and pushed the two halves of the droplet

in opposite directions. There is a small likelihood that the unsteady nature of the fountain could have pushed individual droplets back and forth retracing their paths.

Flat-Plate Wing/Body Combination

Figure 9 shows the typical undersurface flow pattern for the flat-plate wing/body combination for an NPR of 1.5 and a nozzle height of 3.48 in. ($H/D_e = 2$). The flow is dominated by the outflow from the fountain impingement line which can be seen together with some of the same features discussed in the flat-plate body alone results.

Interestingly, the fuselage forward of the front jet, aft of the rear jet, and along the wing trailing edge demonstrates low flow velocities (shown by the undisturbed paint dots). Adjacent to these regions, apparently the fountain flows are flowing downward away from the fuselage surface into the spanwise vortex flow sketched in figure 1(a). In contrast, the wing leading edge is in the region of these vortices and experienced many droplets flowing around or off the surface (including some droplets from the second and third rows back). The wing leading edge flow is apparently dominated by the upward flow from the fountain and the resultant vortex pair.

Round Body Alone

Figure 10(a) shows the undersurface flow pattern for the round body alone for an NPR of 3.0 and a nozzle height of 10.44 in. ($H/D_e = 6.0$). A side view of the model is shown in figure 10(b). The 3-D effects of the contoured model are very apparent. The flow from the two spanwise vortices formed between the fountain and the jets shows a larger lateral flow magnitude near the fountain stagnation point. The flow seems to be seeking a path along the surface of the body and it is not constrained to a fore-aft flow pattern as was the case with the flat body. Therefore the flow pattern is symmetric about the single point defined by the fountain impingement on the bottom of the fuselage. Again notice that some of the droplets forward of the front nozzle and aft of the rear nozzle did not appear to move, indicating low to no flow velocity.

Round Body/Low-Wing Combination

Figure 11 shows the undersurface flow pattern for a round body/low-wing combination at an NPR of 3.0 and a nozzle height of 6.96 in. ($H/D_e = 4.0$). As was expected, the flow patterns for the round body/low-wing configuration and the flat-plate body/wing combination are very similar. The 3-D flow pattern that would have formed due to the contoured body is halted by the flat wing.

Since no obvious effect of either the NPR or the nozzle height on the direction of the surface streamlines was seen in any of the models discussed so far (flat-plate body, flat-plate wing/body combination, round body alone and round body/low-wing combination) these photographs are not presented. Common features for all of the photographs include the undersurface stagnation line in the middle of the distance between the two nozzles and the jet-induced entrainment of the flow into the jets from the low pressure region around the nozzles. Outboard of the nozzles, as shown near the wing trailing edge, the paint shows that the flow is turned downward into the rear vortex near a lateral line through the jet center. Across the wingspan the lower wing surface flow turns uniformly toward a direction parallel to the fuselage center.

Round Body/High-Wing Combination

The effects of NPR on the undersurface flow for the round body/high-wing model at a height of 3.48 in. ($H/D_e = 2$) are presented in figures 12(a)–12(h) and at a height of 10.44 in. ($H/D_e = 6$) are presented in figures 13(a)–13(g). These photographs were obtained from runs where the NPR was held constant while the height was varied. For example, figure 13(a) was photographed at $H/D_e = 6$ and figure 12(a) was photographed later when the height was reduced to $H/D_e = 2$. As a result the manually applied paint dot pattern varies through the photographs for figures 12(a)–12(g) where $H/D_e = 2$. These patterns are exactly the same in the corresponding photographs for figures 13(a)–13(g) where $H/D_e = 6$. The two photographs (figs. 12(a) and 13(a)) show the fountain impingement on a red row of dots. Immediately aft of this row on the fuselage centerline (fig. 13(a)) is a dot of blue paint which appears to be larger than adjacent dots. It ran toward the right side of the fuselage. In figure 12(a) this same dot may be seen to run even farther. Similar comparisons of flow anomalies for selected paint dots may be seen for parts (a) through (g) of both figures 12 and 13.

The jet-induced fountain impinges the lower surface of the wing-body at a location midway between the jet exits and forms a spanwise stagnation line. The fountain impingement line on the undersurface of the model can be seen wrapping around the fuselage and extending laterally on each side of the wing surface, all the way to the leading edges. The effect of the inlet duct mounting brackets can be seen in the photographs. As the upwash flow wraps around the fuselage it separates at the sharp edges of the brackets, probably forming a separation vortex along the length of each bracket. These vortices bring the

flow toward the wing lower surface and form chordwise reattachment lines on each side of the wing near the 0.4 semispan location. Inboard of the reattachment lines the flow direction is toward the body and wing trailing edge. Outboard of the reattachment lines the flow direction is toward the wing trailing edge and wing tip in a direction roughly parallel to the wing leading edge. There seems to be a relationship between NPR and direction of outboard undersurface streamlines which will be discussed later.

Figure 14 shows the undersurface flow patterns for the round body/high-wing combination with side inlets. The inlets were not sucking air. The nozzle height was fixed at 3.48 in. ($H/D_e = 2$) while the NPR was varied from 1.5 to 6.0. The inlet ducts, 1.5 in. in diameter, provide a surface outboard of the duct mounting brackets between the wing and the upwash flow. The inlets were not sucking air. The inlets caused the reattachment lines on the wing to move farther out, as one might expect, to a chordwise line near the 0.55 semispan location. There is a downward flow on the side of the model fuselage between the inlet duct and the wing lower surface shown in figure 14(b). This confirms a vortex structure in this narrow, thin area. The forward flow of this vortex can also be noted toward the front on the fuselage as it spills past the inlet face. There are no corresponding flow patterns in the aft region near the wing trailing edge. The lack of aft flow of this vortex at the wing trailing edge indicates again that the flow is being drawn downward into the vortex pair induced by the fountain.

The data for the configuration without inlet ducts which are presented in figures 12 and 13 show that as NPR increases there is a variation in wing undersurface flow direction outboard of the chordwise reattachment lines. In contrast, the data presented in figure 14 show very limited variation in undersurface flow direction due to NPR variation. As an indication of these changes, the angle Φ of the local streamlines near the 2/3 semispan location was measured with respect to the fuselage centerline. These angles are presented in figure 15 as a function of NPR. There are two comparisons shown in the figure. When there is no inlet duct, the flow angle Φ decreases from over 20 deg at an NPR of less than 3, to less than 10 deg at an NPR of 4.5, and then increases to over 30 deg at an NPR of 6. The change in height from 2 to 6 effective diameters has virtually no effect. However, when the inlet duct is present below the high wing, the flow angle Φ is nearly constant at 8 deg with a few degrees variation over the range of NPR tested. These data emphasize how sensitive the ground-induced flow characteristics are to aircraft configuration changes.

Concluding Remarks

A flow visualization study was conducted on several jet-powered VTOL airplane models to investigate configuration, NPR, and nozzle height effects on the undersurface flow patterns. Little difference was observed among the flow patterns on the undersurface of the flat plate, the 3-D body alone, and 3-D low-wing models. Also, NPR and nozzle height seem to have no effect on the direction of the surface streamlines for these models. All of the low-wing configurations also demonstrated stagnant regions near the wing trailing edge and aft of the rear nozzle as well as forward of the front nozzle. This flow pattern is consistent with flow pattern induced by the vortex pair created between the fountain and the two jets.

A more obvious difference is apparent in the comparison of the low-wing surface flow pattern with those for the high-wing model. The low-wing flow aft of the fountain impingement line tends uniformly toward a direction parallel to the fuselage centerline. The high-wing flow aft and outboard of the fountain impingement line on the lower wing surface flow tends toward a direction parallel to the wing leading edge.

The fountain flow-induced wing undersurface flow angles are very configuration dependent. For example, the NPR can have a large effect on the direction of the undersurface streamlines especially for the high-wing configuration without inlet ducts. In particular, the flow direction at the wing trailing edge near the 2/3 semispan location changes from about 20 deg at low NPR, to a minimum of about 5 deg at an NPR of 4.5, and up to about 30 deg at an NPR of 6. In contrast, this angle is nearly invariant (about 8 deg) with change in NPR when the inlet duct is mounted below the high wing.

Appendix—Photographic Procedure for Oil Flow Visualization

This appendix describes the techniques and the equipment used to take the photographs presented in this report. This description has been abstracted from a more detailed report prepared by the photographers, Tom Reddy and Dominic Hart.

The objective of this test was to photograph fluorescent oil and tufts on the model using ultraviolet (UV) filters on the light source, more commonly known as black lights. To better illuminate the model, flash units were necessary. Because the UV filters absorb so much light, the output from each flash head had to be high.

In the tests the primary variable was model height. Height changes were achieved by moving the ground plane vertically relative to a fixed model from a distance of 54 in. to a distance of 3.5 in. To obtain photographs of the bottom of the model lower surface, a camera was mounted in the ground plane with a transparent plastic surface. The camera was selected to be able to still show all (or most) of the model in the frame. For the same reasons, light stands could not be positioned very close to the platform because of the varying clearance between the platform and the model. For safety reasons, people were not allowed in the test area while the air was blowing so the camera was triggered remotely from the control room (a distance of about 50 ft).

Equipment and Supplies

A partial list of the equipment and supplies used is listed below:

- one 35 mm auto focus camera (Nikon F4) with time code capabilities
- one 20 mm auto focus lens f/2.8 (Nikon)
- two Hassleblad ELM bodies
- two Hassleblad A12 film magazines
- one 250 mm lens (Hassleblad)
- one 80 mm lens (Hassleblad)
- one 50 mm lens (Hassleblad)
- four Norman LH2000 fan cooled lamp heads
- four non-UV-coated flash tubes
- four 6 in. round black light filters
- film: Kodak VPH ASA 400, Kodak T-Max 400, 120, and 135 format

Setup Procedure

1. Setup of camera one, auto focus, 35 mm with the 20 mm lens

A small tripod was placed on the scissor lift directly under the Plexiglas window. Camera one was set to print the hour/minute/second on the film and the frame count outside the frame. The camera was loaded with T-Max 400 film for an exposure test. The camera was set to manual mode at 1/125 second shutter speed and started at the maximum f stop for the film test, stopping down one stop for each of the following exposures. The camera was then attached to the tripod. The receiving unit of the radio slave was placed next to the tripod and the cord was attached to the camera. The antenna was placed so that it would not touch any metal (it was taped to a plastic part of the tripod so it would not move during the test); otherwise, misfires or nonfires would occur. The multiple synchronization plug was placed into the camera and then two 12 ft synchronization cords were run from the plug to either side of the test platform (these were later attached to the power packs).

2. Setup of the Hassleblad cameras two and three for side views

A second camera was located in a fixed location at the height of the nonmoving model to obtain a model side view. A third camera was set up on a tripod located farther from the test area to show a side view of the entire area. A motor driven film advance was needed because the camera was inside the test area. Since the model was suspended 12 ft off the ground the camera was mounted on a tripod located on a tall, stable platform. Once the camera was on the platform, the 250 mm lens was focused on the model. The radio slave was set up next to the camera and the cord was attached. A 12 ft synchronization extension cord was run from the camera to the platform. This was later attached to two other cords and then to the power packs. The shutter speed was set to 1/125 second and the aperture was set wide open to start the film test. The film pack was loaded back with T-Max 400 film and placed on the camera.

3. Setup of the flash heads to hold the UV filters

An adaptor was built to fit filters to the flash heads. Four 6 in. × 4 in. strips were cut out of a thin sheet of aluminum. The aluminum was then twisted into circle tubes the size of the flash head and carefully taped to form the adaptors. The adaptors were made taller than the flash tube so the filters would not rest on the flash tubes. Finally, the filters were placed on the aluminum tubes and held in place with safety wire. If the modeling light is

accidentally left on, the heat would damage the flash head. Therefore the modeling light was taken out of each of the lamp heads to prevent overheating because the UV filters transmit only the ultraviolet light while all other wavelengths stay inside, including infrared heat.

4. Mounting of the flash unit to the A-frame

The flash units were mounted on the A-frame surrounding and supporting the test model to ensure the light stands were not in the jet-induced flow. Three flash heads were placed on the A-frame and one was attached to a boom arm mounted to the A-frame. Three large C-clamps and three metal dowels machined to fit into the flash head were used. Two areas on the dowel were flattened to fit securely between the A-frame and C-clamp. When attached to the A-frame, the flash heads were positioned high enough to provide light between the platform and the model when the platform was at its closest point.

5. Setting the power packs and synchronization cords

Four Norman P2000 power packs were used, one for each light, two on each side of the A-frame. The power setting for each light was 2,000 watts. Two power packs were plugged into one outlet on one side of the building and two at the other end. Separating the packs reduced the chance of a blown circuit. Because of condensation during the test run, plastic bags covered the power packs to keep them from getting wet. Each camera had two flash heads and two power packs. The synchronization cords were attached to the power packs allowing each camera to have one flash head on either side of the A-frame.

Film Test

For the film test, T-max 400 film and VPH film rated at ASA 400 were used. Initially, the apertures were set wide open on both cameras. An exposure was made using each camera and its corresponding power packs. Cameras one and two were stopped down one stop and another exposure was made. The process was repeated until the smallest aperture on both cameras was reached. The film was processed and analyzed to see which apertures worked best with each film and camera combination.

The results showed that on camera one, f/4 worked well for both black and white and color. F/5.6 gave a good exposure on cameras two and three. The apertures were set and remained the same for the duration of the test. The exposure was set at 1/125 second for both cameras two and three.

Comments

The images were clear and the information from the oil flow showed up as brilliant and vibrant colors. They gave an accurate display of the flow around the airplane model. The background fluorescent safety light used for the 35 mm gave a green cast to the side of the model and, in some cases, it put a bright highlight on the model. It was necessary to have it on at all times, but the use of a magenta filter over it, as well as the flash units, would have cut down on the green cast and helped in the color balance and exposure.

Visualization of the flow in the region of the nozzles was made possible by shining UV light on the paint/oil drops painted on the model. The first camera, located in the ground plane, was auto focus because of the 50.5 in. distance it moved during the runs. Even at the close distances to the model, the image was still in focus, which would have been impossible with a standard manual focus camera. The use of four 2,000 watt power packs for the flash heads was also a necessity because of the intensity loss with the filters and the distance from the subject. Setting the exposure at f/4 resulted in a better depth of field and showed the entire model in focus. A second camera was located in a fixed location at the height of the nonmoving model. A third camera was set up on a tripod located farther from the test area to show a side view of the entire area. This camera was able to show the visible air blown out of the nozzles in ground proximity. For the exposure, a long shutter release cable was used to manually open and close the lens. When it was time to expose the other two cameras, the shutter was opened for normal exposures. Cameras one and two fired their own strobes; the third camera, whose lens was open, was exposed in the process. Its lens was then closed and the camera would automatically advance the film for the next exposure.

References

1. McLemore, H.; and Smith, Charles C., Jr.: Hot-Gas Ingestion Investigation of Large-Scale Jet VTOL Fighter-Type Models. NASA TN D-4609, 1968.
2. McLemore, H. Clyde; Smith, Charles C., Jr.; and Hemeter, Patricia G.: Generalized Hot-Gas Ingestion of Large-Scale Jet VTOL Fighter-type Models. NASA TN D-5581, Jan. 1970.
3. Williams, John; and Wood, Maurice N.: Aerodynamic Interference Effects With Jet-Lift V/STOL Aircraft Under Static and Forward-Speed Conditions. Tech. Rep. No. 66403, Brit. R.A.E., Dec. 1966.
4. Lavi, Rahim; Hall, Gordon R.; and Stark, Wilbur W.: Full-Scale Ground Proximity Investigation of a VTOL Fighter Model Aircraft. NASA CR-1098, 1968.
5. Hall, Gordon R.; and Rogers, Kenneth H.: Recirculation Effects Produced by a Pair of Heated Jets Impinging on a Ground Plane. NASA CR-1307, 1969.
6. Kirk, Jerry V.; and Barrack, Jerry P.: Reingestion Characteristics and Inlet Flow Distortion of V/STOL Lift Engine Fighter Configurations. AIAA Paper 68-78, Jan. 1968.
7. Ryan, Patrick E.; Heim, Richard J.; and Cosgrove, Wayne J.: A Generalized Experimental Investigation of Hot Gas Recirculation and Ingestion for Jet VTOL Aircraft. NASA CR-1147, 1968.
8. Abbott, W. A.: Estimation of Intake Temperatures During V/STOL Operation from Model Tests. NGTE Note NT.600, March 1966.
9. Behnert, R.: Untersuchung zur Ahnlichkeitsmechanik von Heissen und Kalten Strahlen und Strahlgruppen, Insbesondere zur Simulation im Modelversuch (Studies of Simulitude Mechanics of Hot and Cold Jets and Jet Groups, Particularly of Simulation in Model Investigations). VFW-Fokker Ea 246 ZTL FAG 4, 1970.
10. Behnert, R.; and Roekmojoto, R.: VAK Dockumentetion Rezirkulation und Strahlinduktion (Recirculation and Jet Induced Effects). VFW-Fokker, 1973 (translated, NASA TT F-15,932).
11. Strock, T. W.; Amuedo, K. C.; and Flood, J. D.: Hot Gas Ingestion Results of a Four-Poster Vectored Thrust STOVL Concept. NASA CR-182115, June 1988.
12. Gray, L; and Kiesielowski, E.: Practical Engineering Methods for Predicting Hot Gas Reingestion Characteristics of V/STOL Aircraft Jet-Lift Engines. NASA CR-111,845, Feb. 1971.
13. Barron, W.; and Frauenberger, H.: Ground Footprint Theoretical and Experimental Studies. Proceedings of Prediction Methods for Jet V/STOL Propulsion Aerodynamics, NAVAIR Workshop, July 1975, pp. 334–357.
14. Green, Kenneth A.; and Zanine, Joseph J.: Computerized Method for an Estimate of Hot Gas Reingestion for a VTOL Aircraft at the Conceptual Design Stage. NADC 78256-60, Aug. 1979.
15. Green, Kenneth A.; and Zanine, Joseph J.: REINGST—User's Manual. NADC 80225-60, Jan. 1981.
16. Green, Kenneth A.; and Zanine, Joseph J.: Estimation of Hot Gas Reingestion for a VTOL Aircraft at the Conceptual Design Stage. SAE SP 591—VSTOL: An Update and Overview, Oct. 1984, pp. 51–66.
17. Mourtos, Nikos J.; and Margason, Richard J.: Evaluation of a Prediction Method for V/STOL Aircraft Hot-Gas Ingestion. NASA TM-103828, Jan. 1991.
18. Bellavia, David C.; Wardwell, Douglas A.; Corsiglia, Victor R; and Kuhn, Richard E.: Suckdown, Fountain Lift, and Pressures Induced on Several Tandem Jet V/STOL Configurations. NASA TM-102817, March 1991.
19. Squire, L. C.; Maltby, R. L.; Keating, R. F. A.; and Stanbrook, A.: The Surface Oil Flow Technique. AGARDOGRAPH 70: Flow Visualization in Wind Tunnels Using Indicators, April 1962.

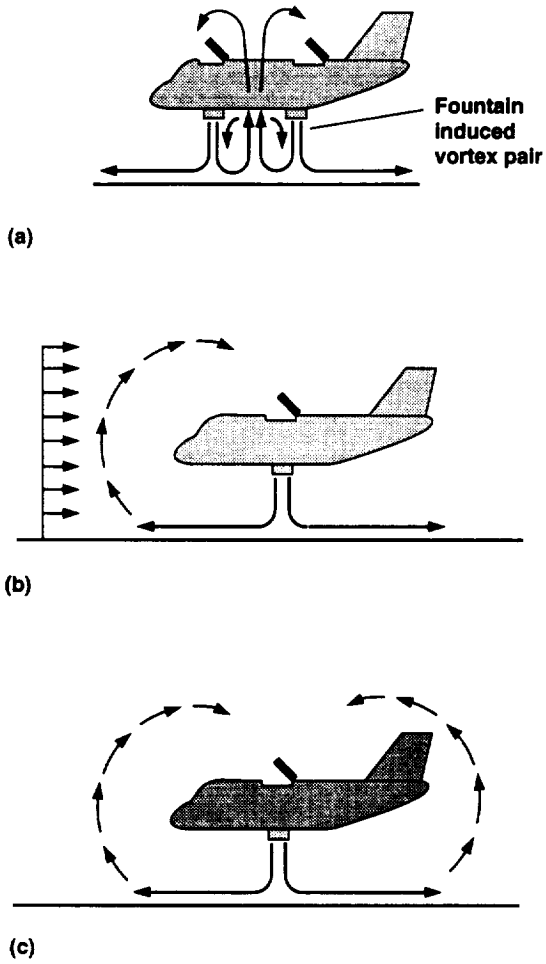

Figure 1. The general flow patterns which cause HGI. (a) Multiple-jet configuration, fountain effect; (b) single-jet configuration, wind effect; (c) single-jet configuration, buoyancy effect.

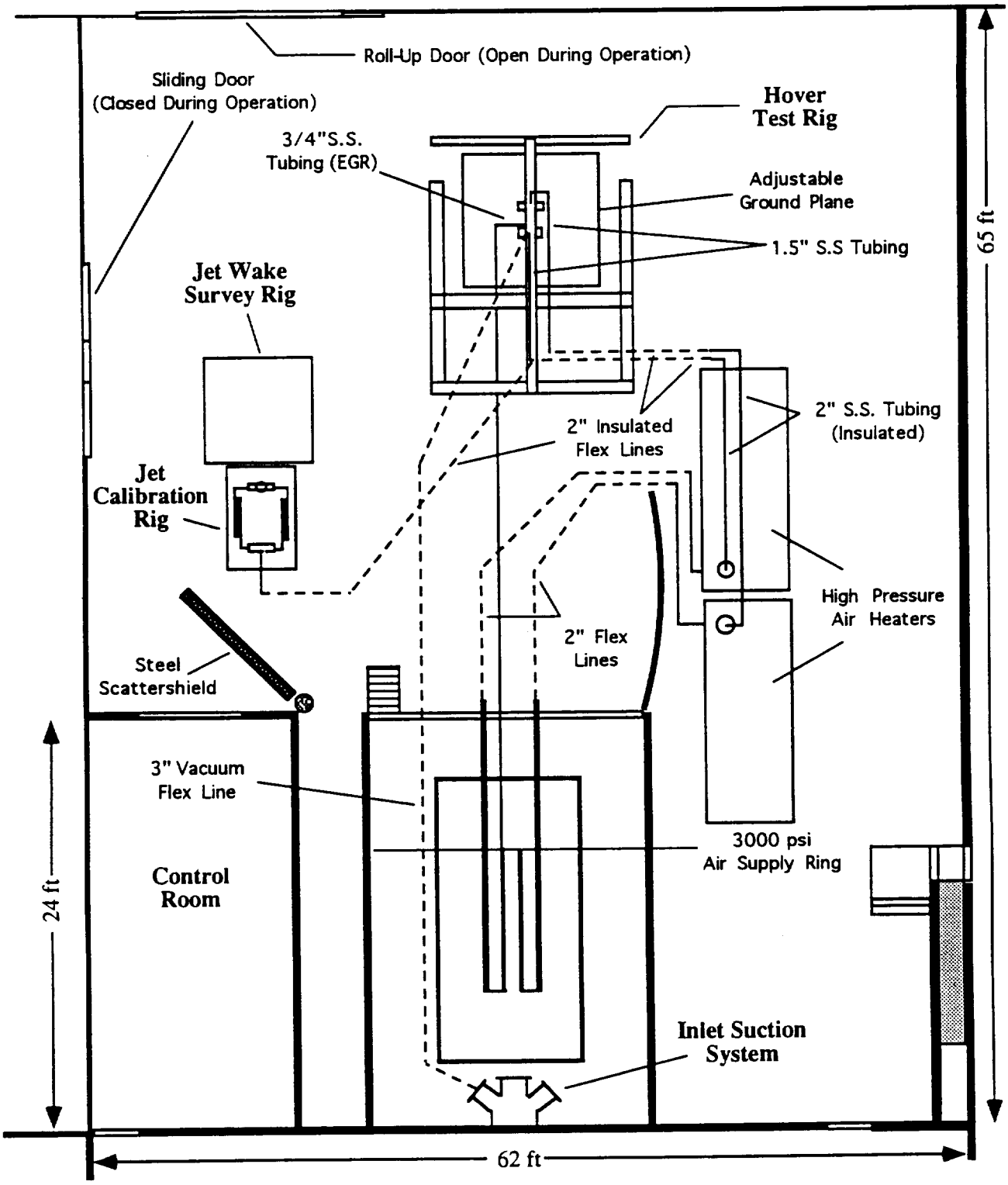

Figure 2. JCAHT Facility/PSCL building arrangement.

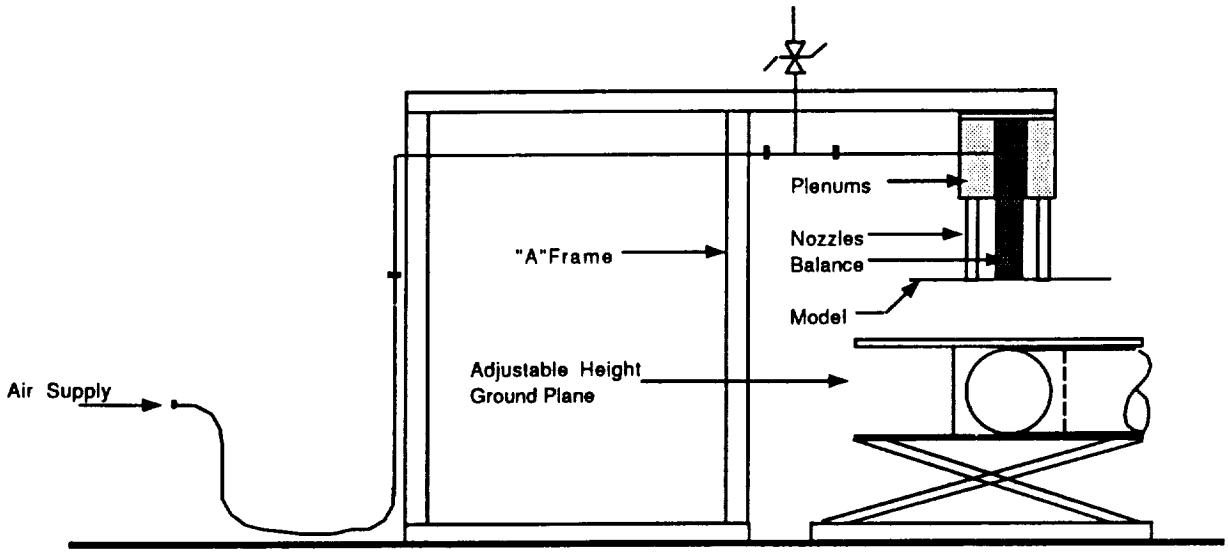

Figure 3. Hover test rig. (a) Schematic sketch.

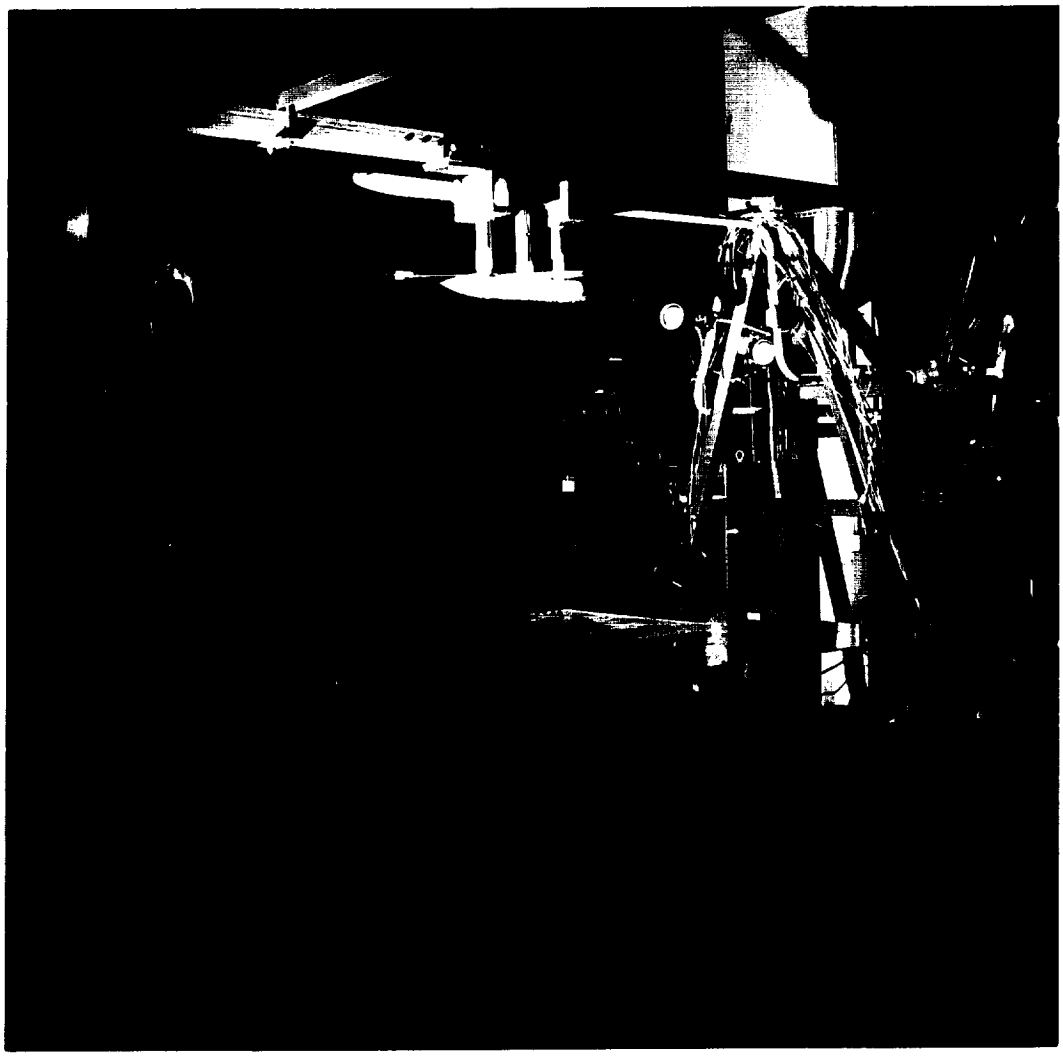

Figure 3. Concluded. (b) HTR showing the high-wing model at H/D_e = 30 and the transparent ground plane.

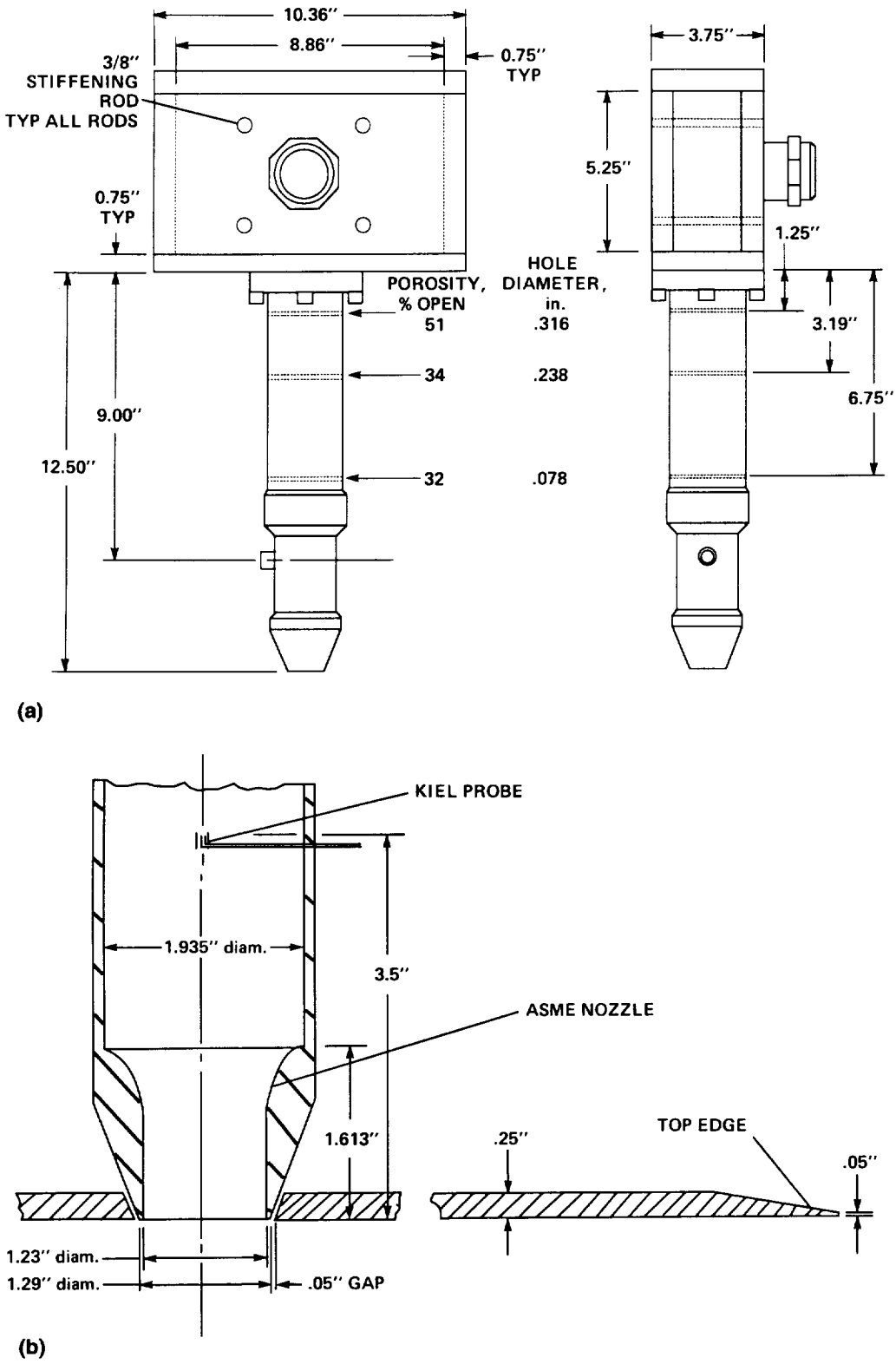

Figure 4. Sketches of nozzle and plenum assembly. (a) Details of the nozzle and plenum assembly; (b) detail of nozzle exit.

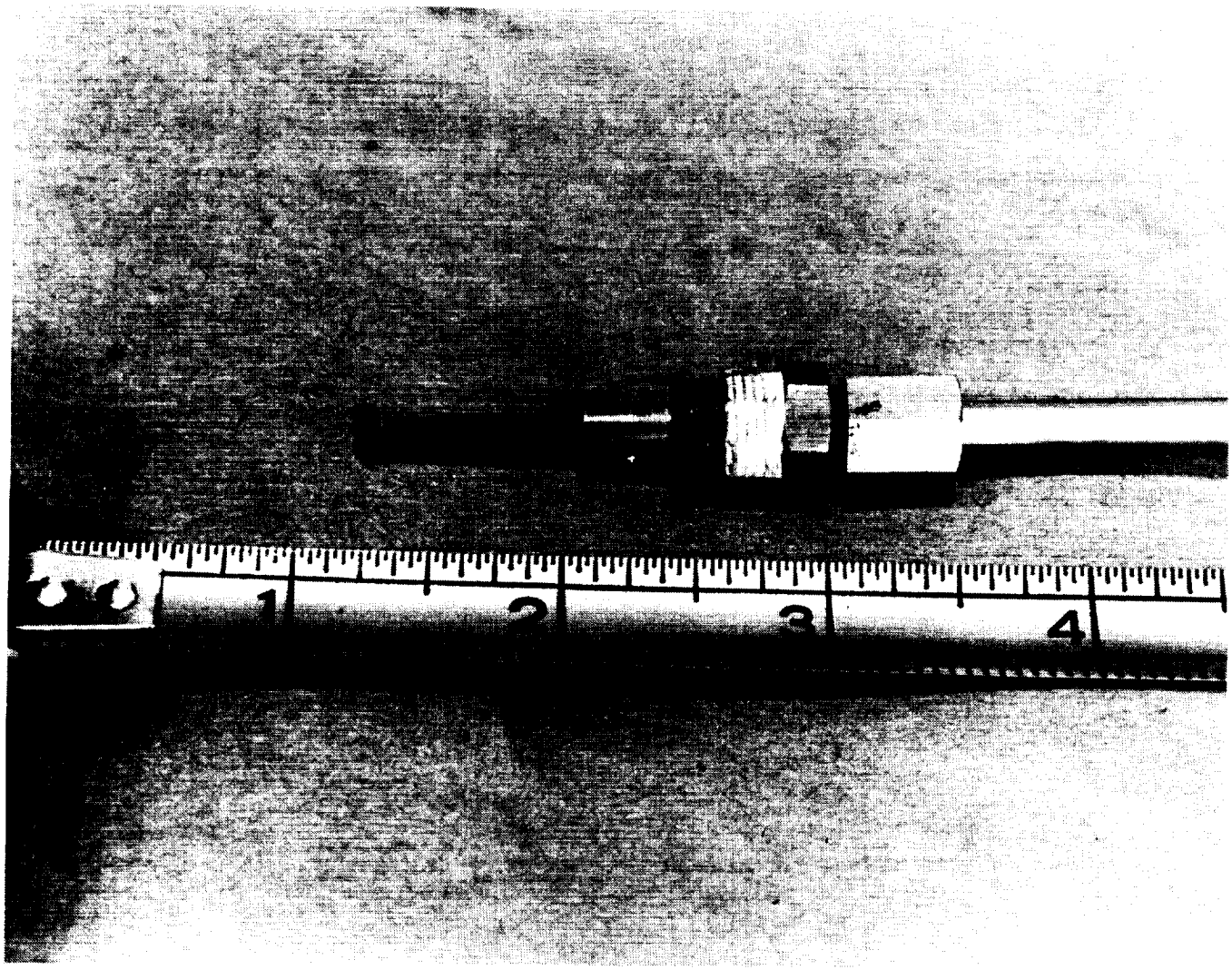

Figure 5. Kiel probe used in nozzle.

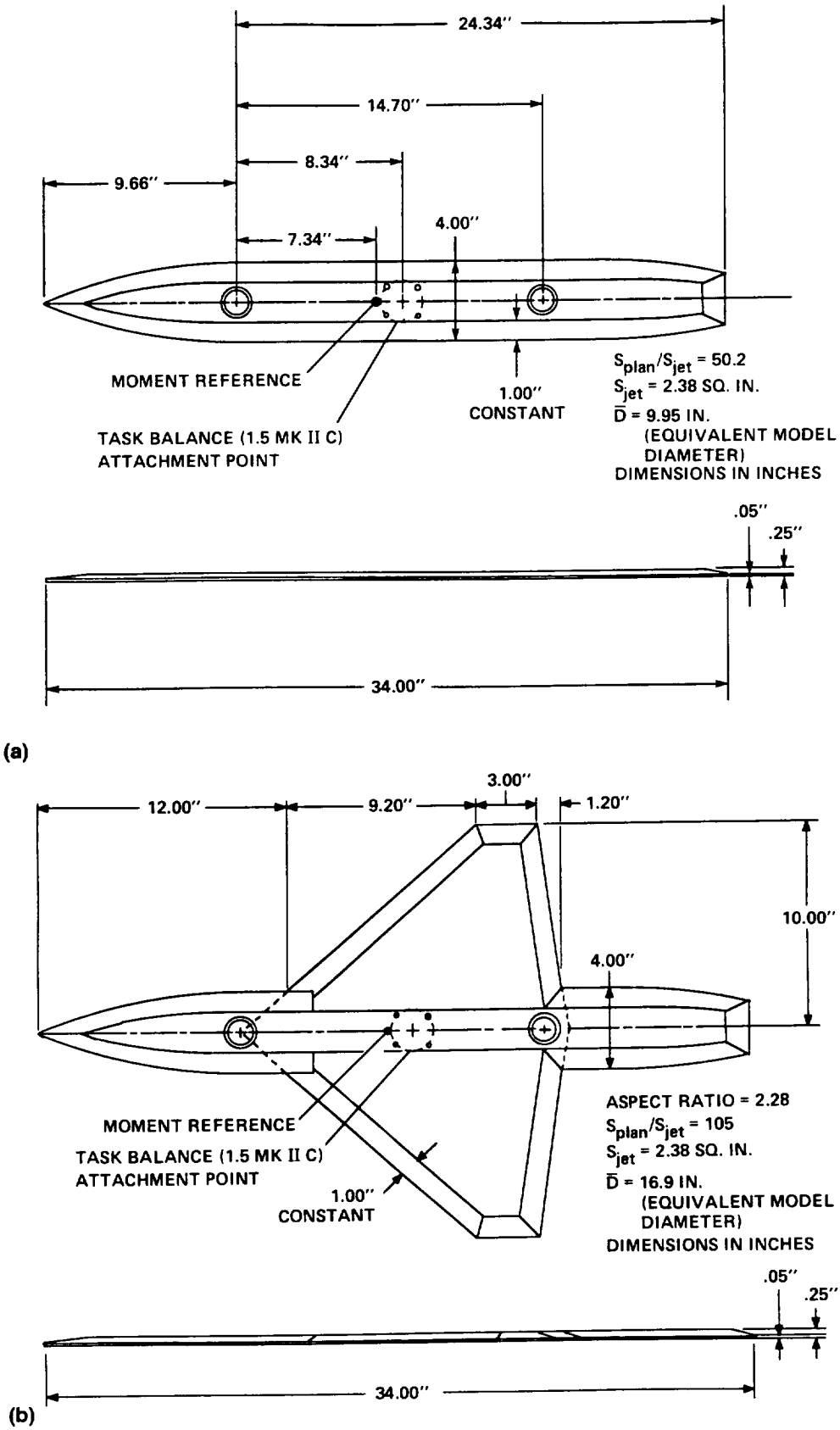

Figure 6. Flat-plate model. (a) Body alone; (b) flat-plate model, wing/body combination.

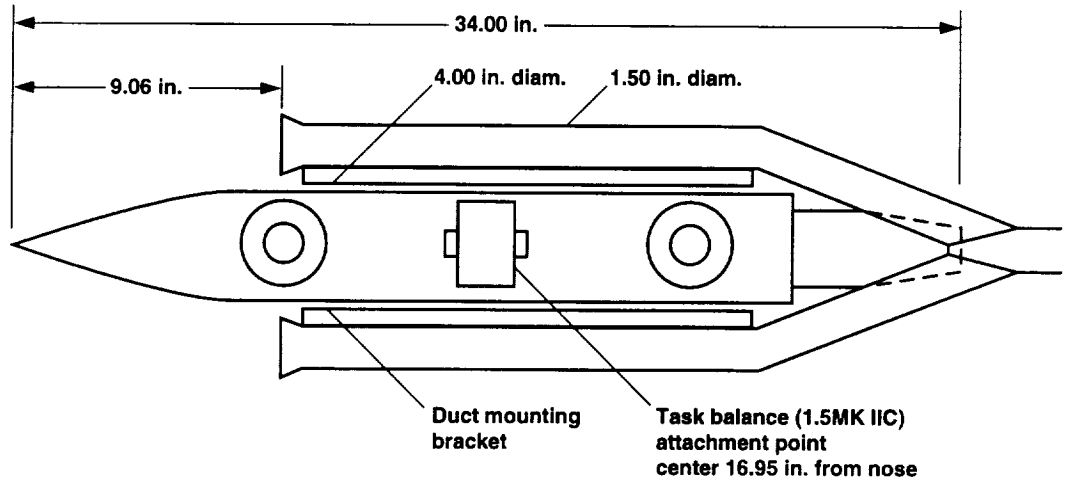

(a)

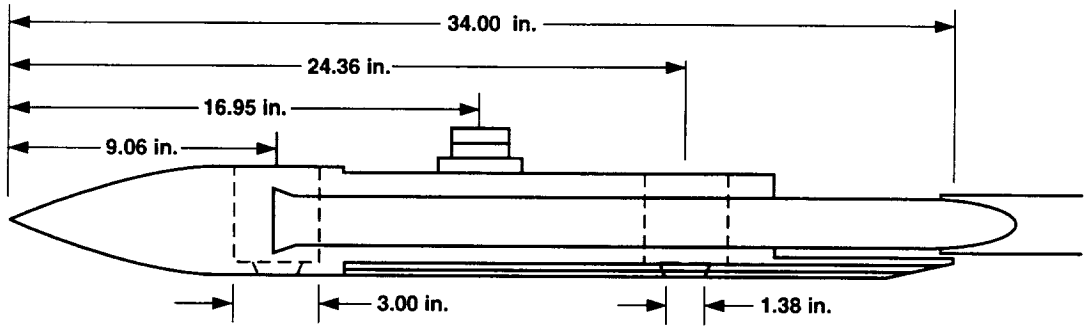

(b)

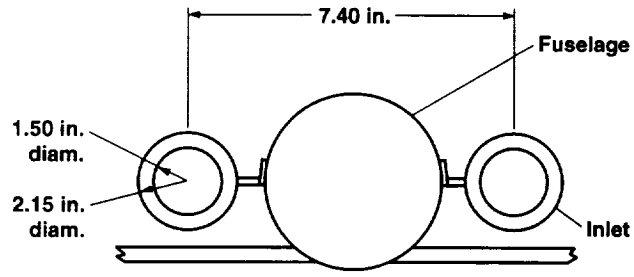

(c)

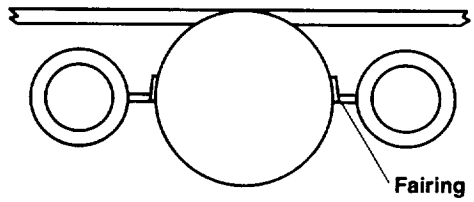

(d)

Figure 7. Three-dimensional round model. (a) Top view of body alone model with side inlets, (b) side view of the body alone model with side inlets; (c) front view of the low-wing model with side inlets; (d) front view high-wing model with side inlets.

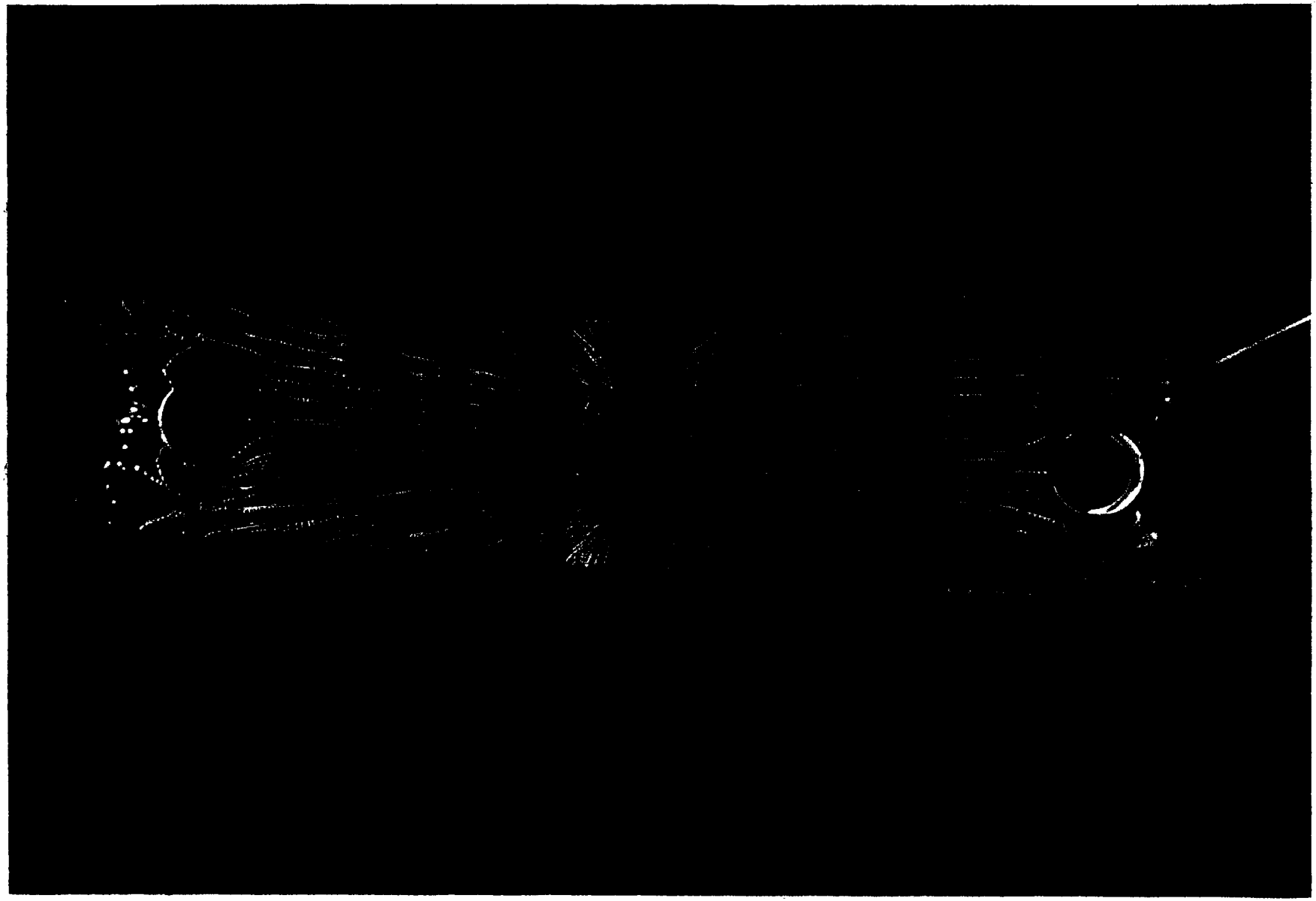

Figure 8. Undersurface flow pattern for the flat-plate body at H = 3.48 in. (H/D_e = 2), NPR = 3.0.

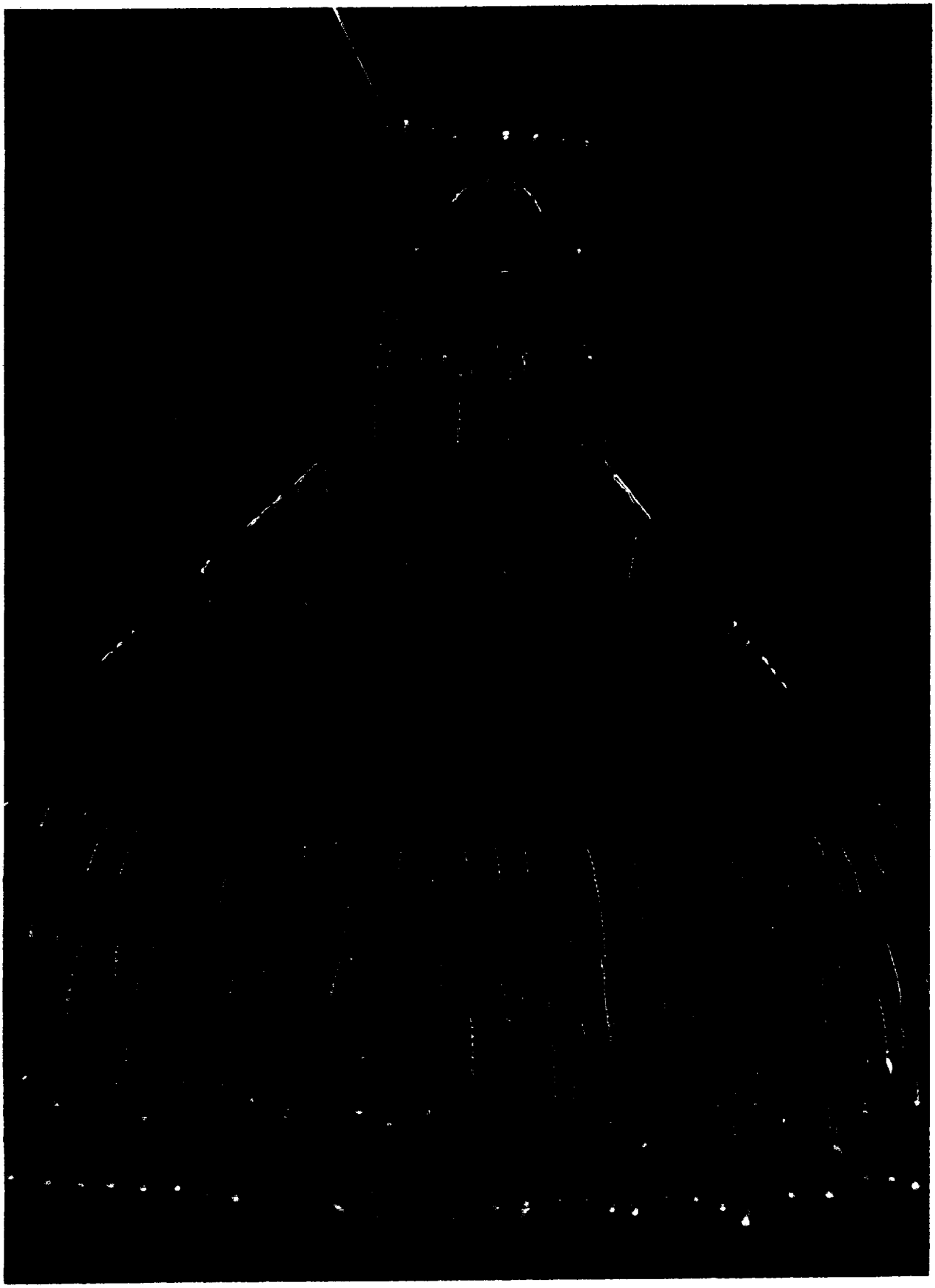

Figure 9. Undersurface flow pattern for the flat-plate wing/body combination at H = 3.48 in. (H/D_e = 2), NPR = 1.5.

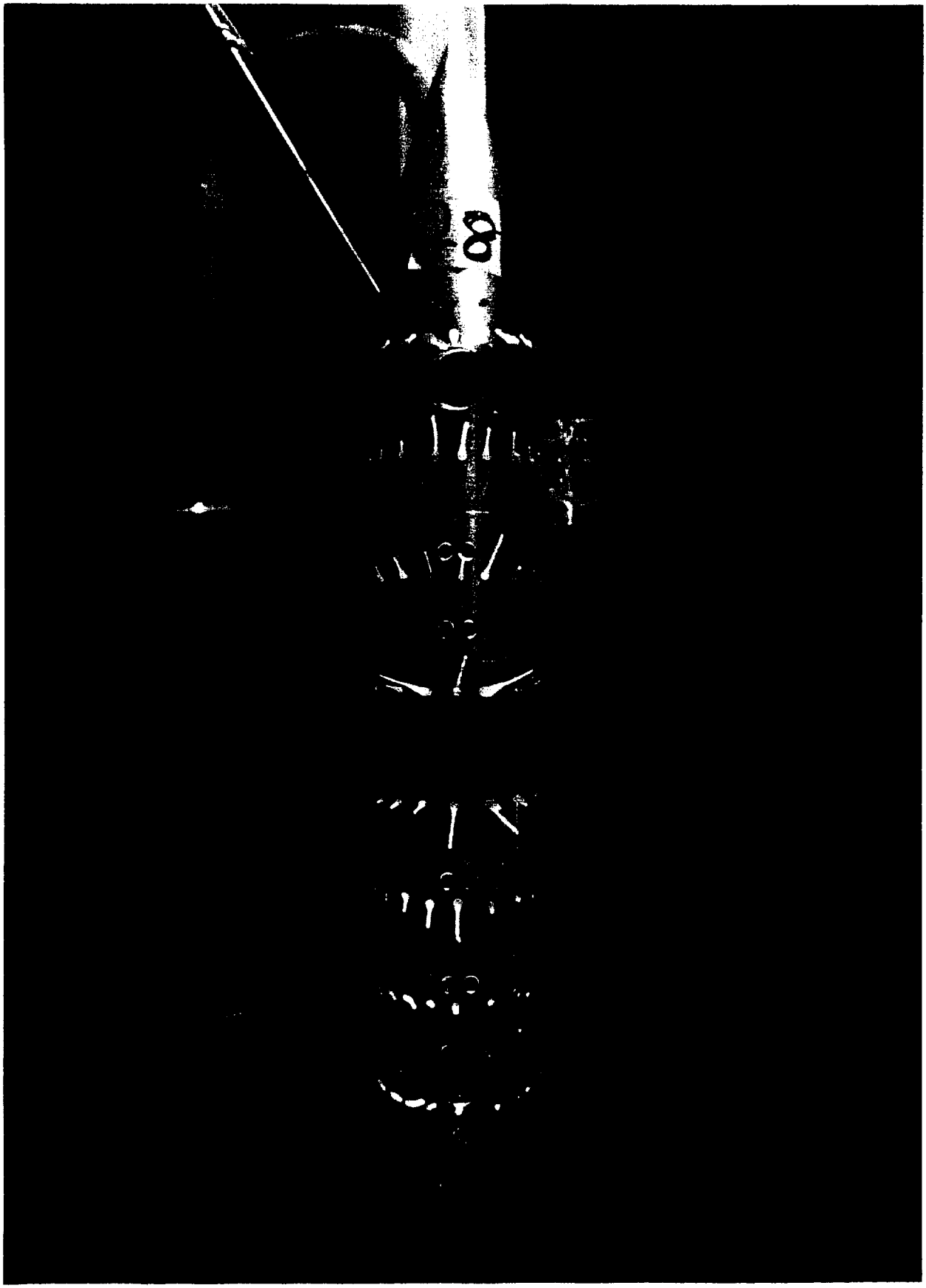

Figure 10. Flow patterns for the round body at H = 10.44 in. (H/D_e = 6), NPR = 3.0. (a) Lower surface view.

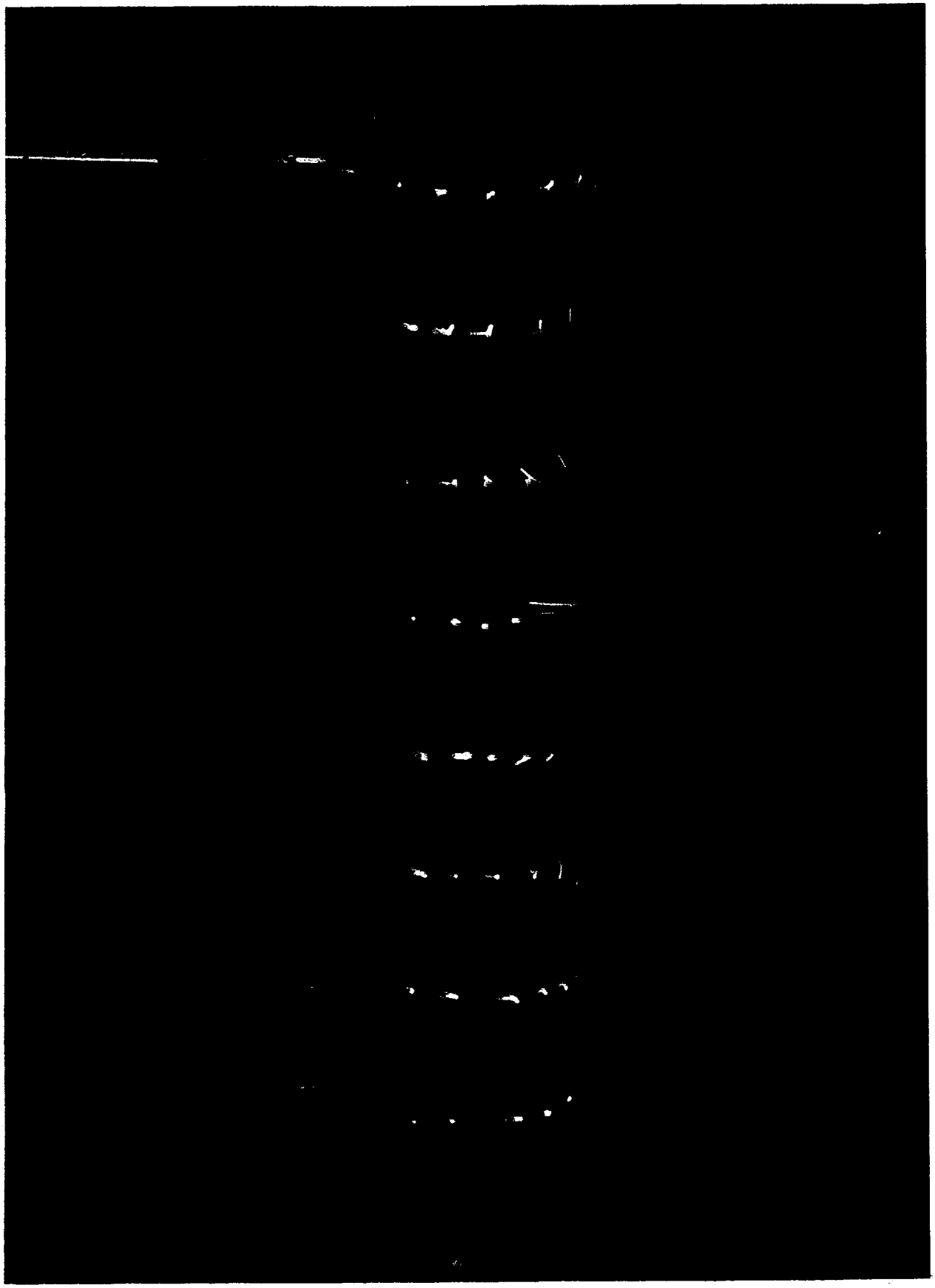

Figure 10. Concluded. (b) Side view.

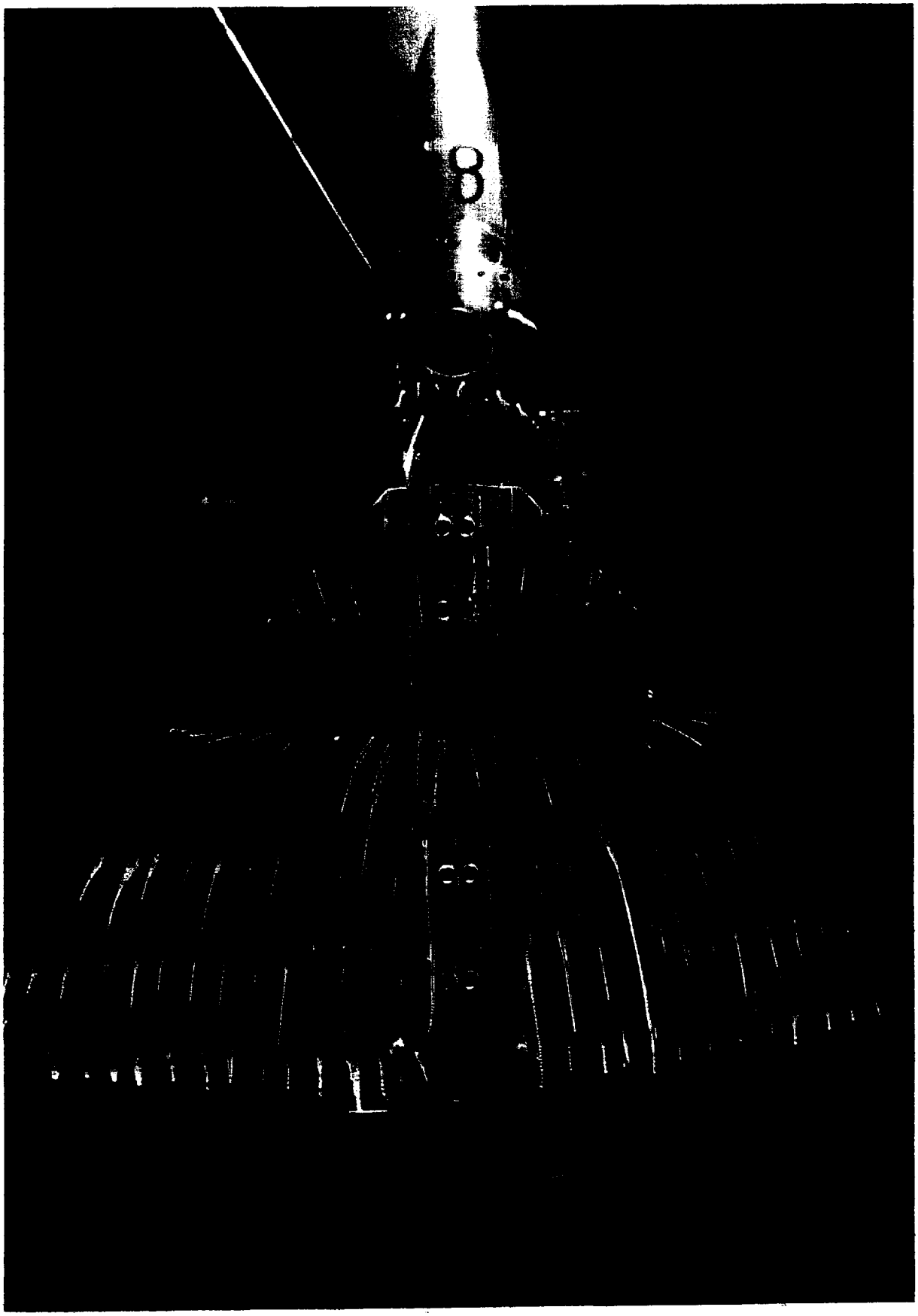

Figure 11. Undersurface flow pattern for the round body/low-wing combination at H = 6.96 in. (H/D_e = 4), NPR = 3.0.

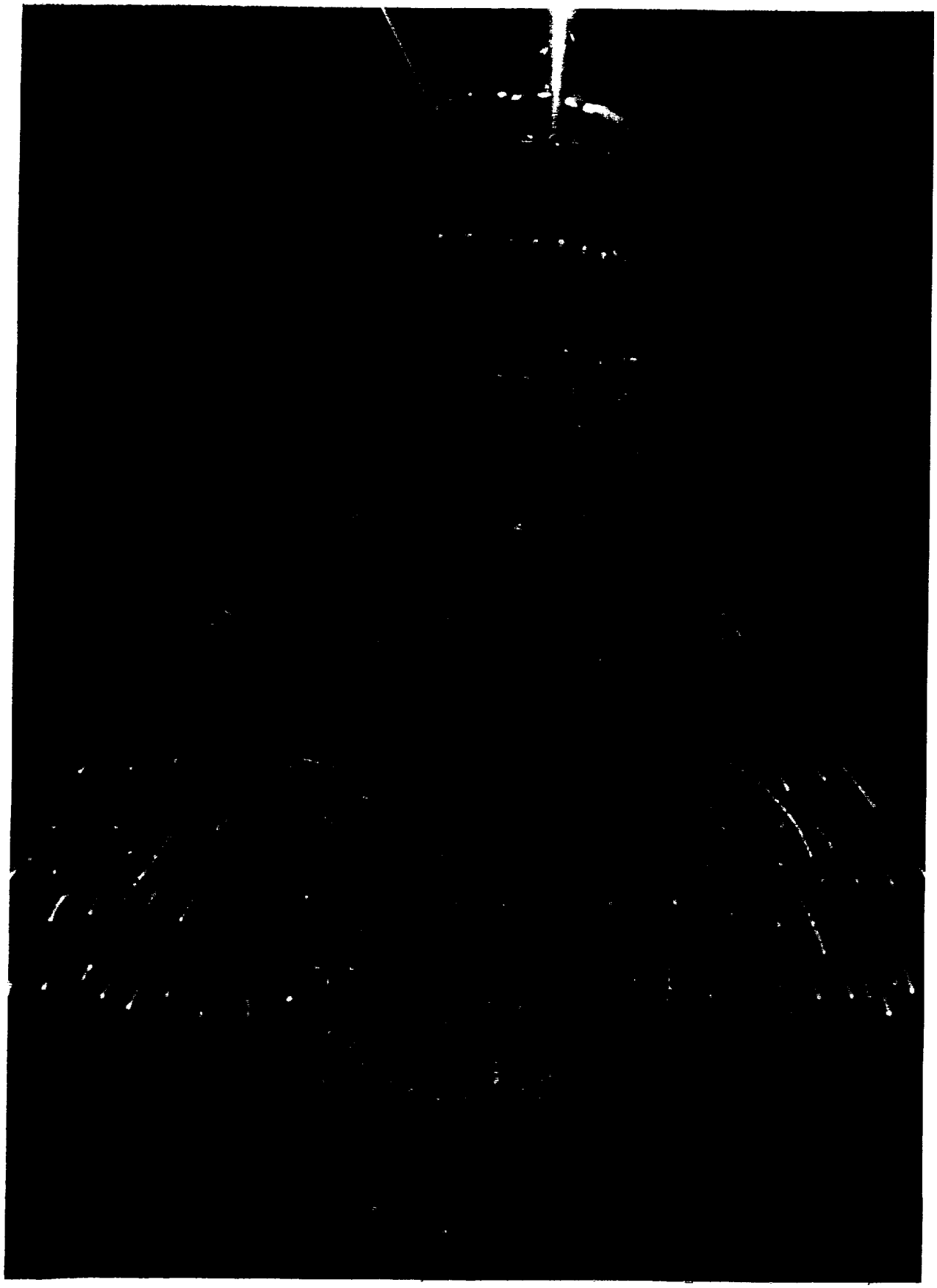

Figure 12. Flow pattern for the round body/high-wing combination at H = 3.48 in. (H/D_e = 2). (a) Lower surface view with NPR = 1.5.

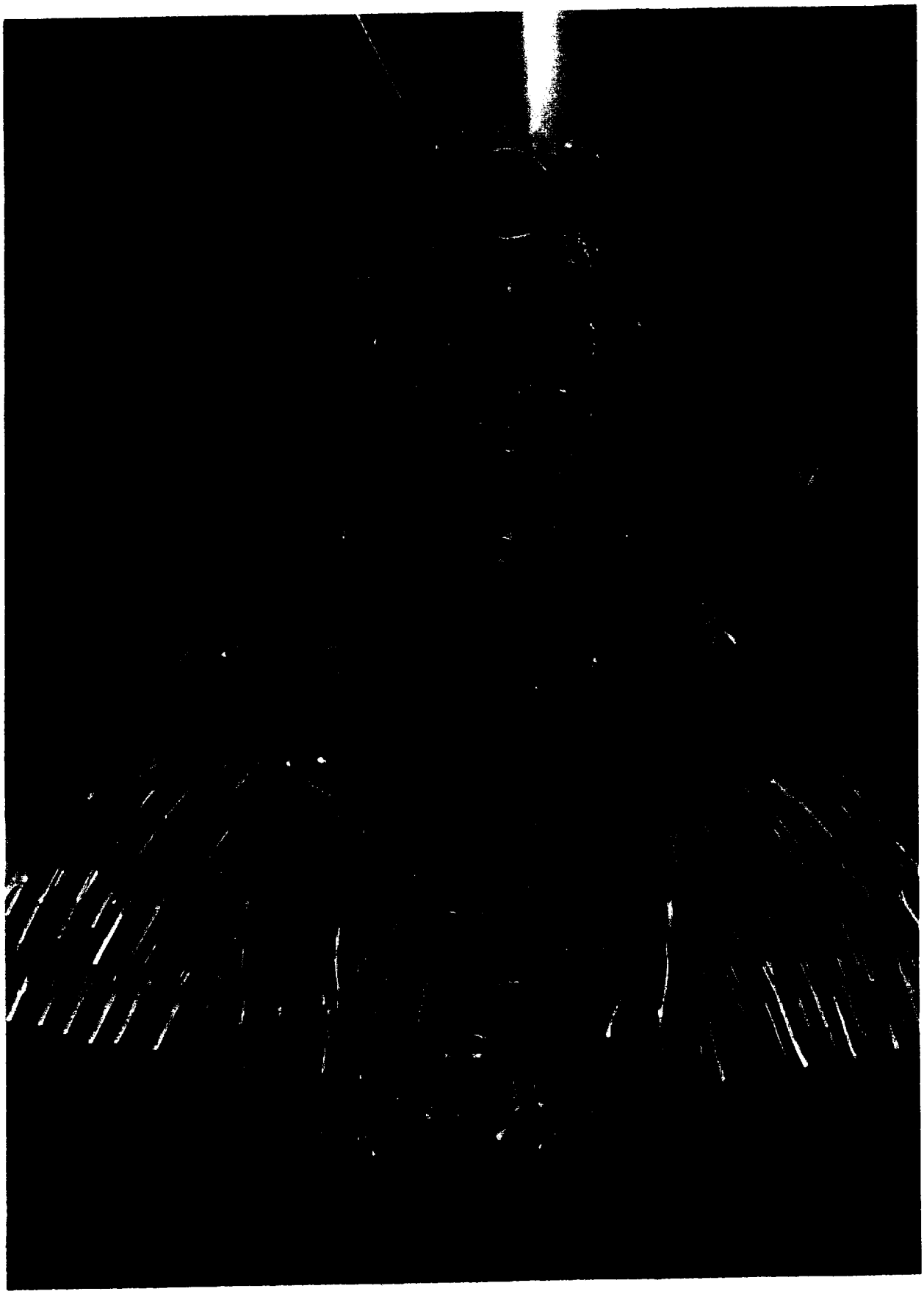

Figure 12. Continued. (b) Lower surface view with NPR = 3.0.

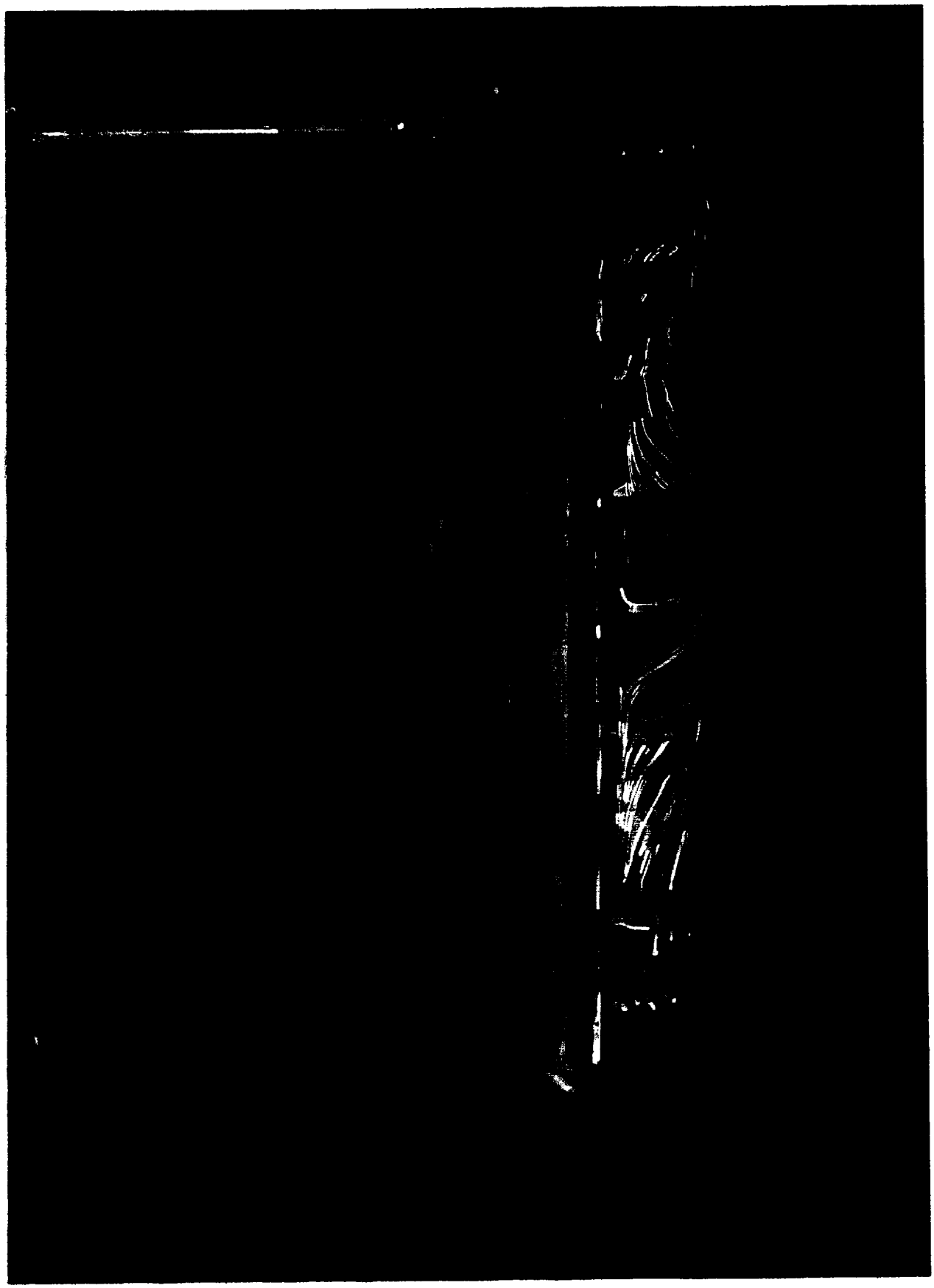

Figure 12. Continued. (c) Side view with NPR = 3.0.

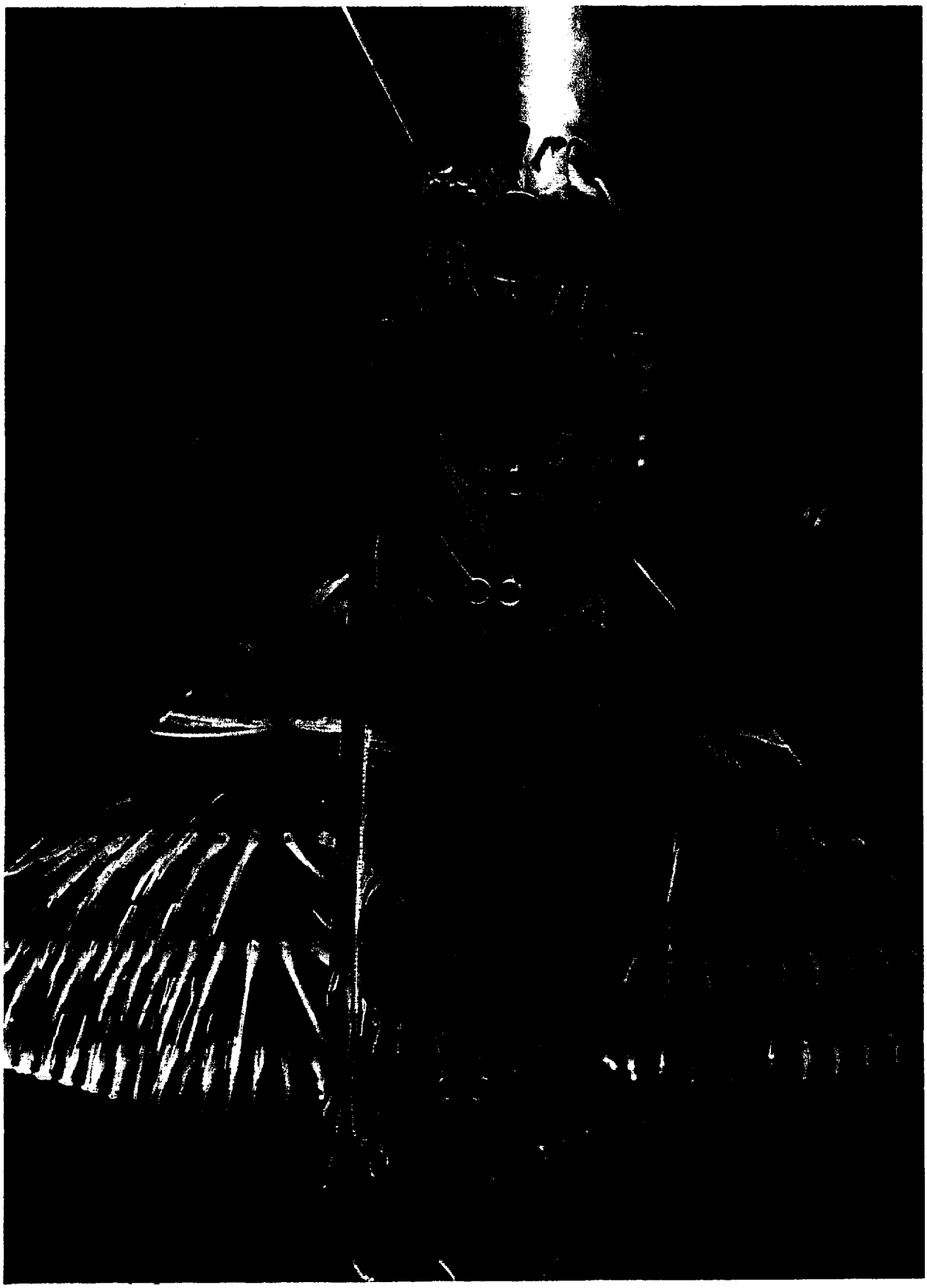

Figure 12. Continued. (d) Lower surface view with NPR = 4.5.

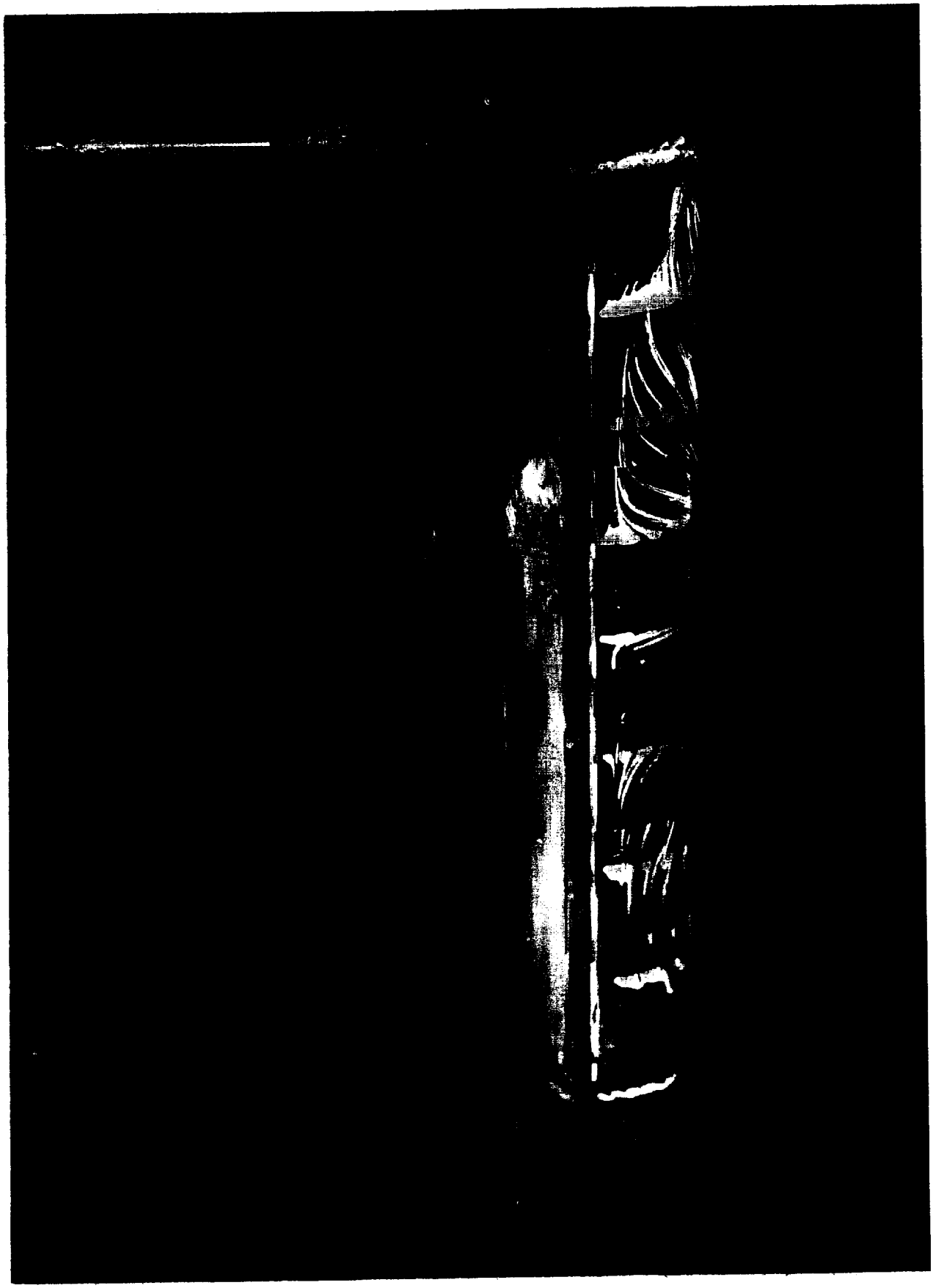

Figure 12. Continued. (e) Side view with NPR = 4.5.

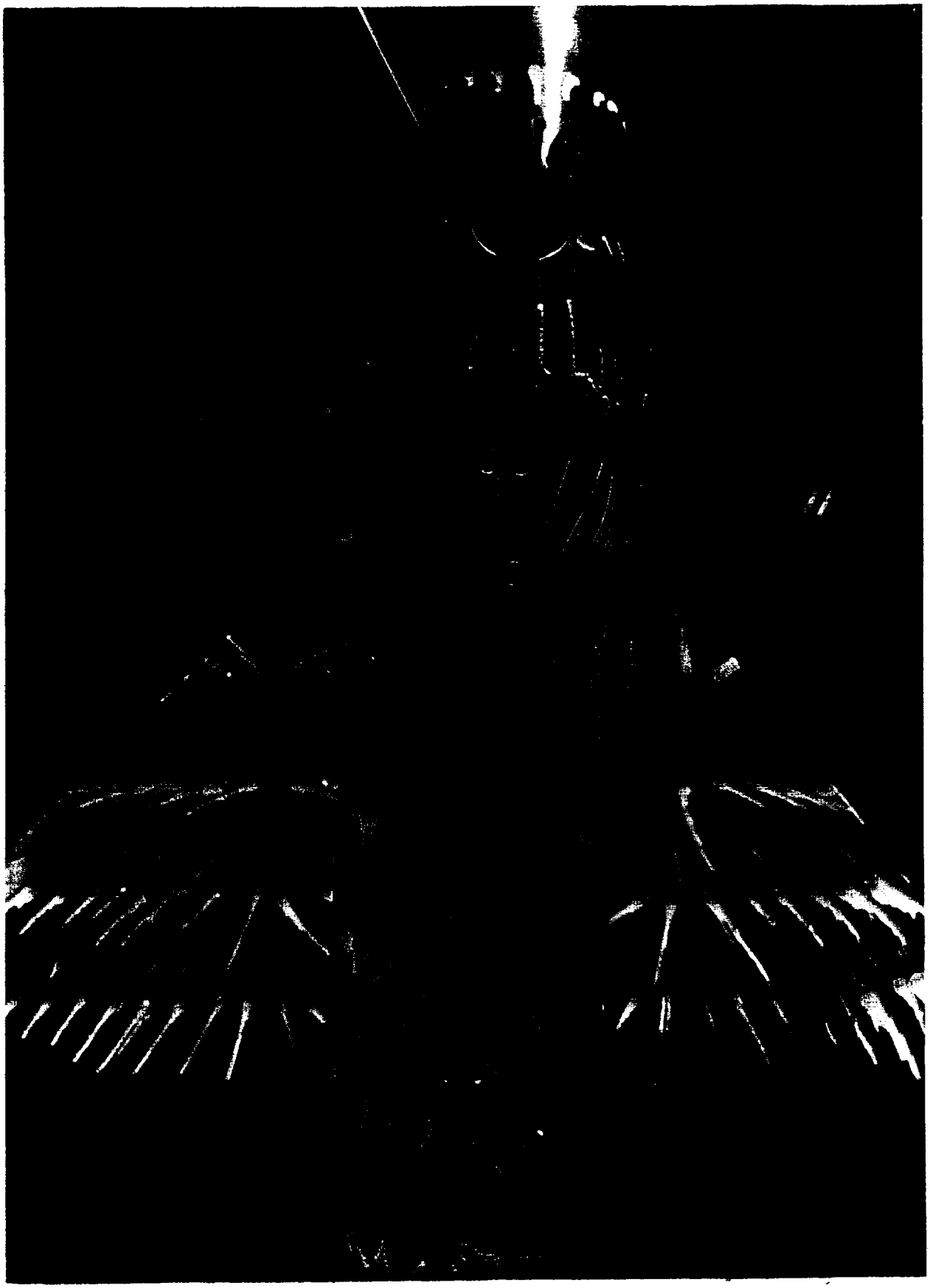

Figure 12. Continued. (f) Lower surface view with NPR = 6.0.

Figure 12. Continued. (g) Side view with NPR = 6.0.

Figure 12. Concluded. (h) NPR = 6.0, wide angle shot.

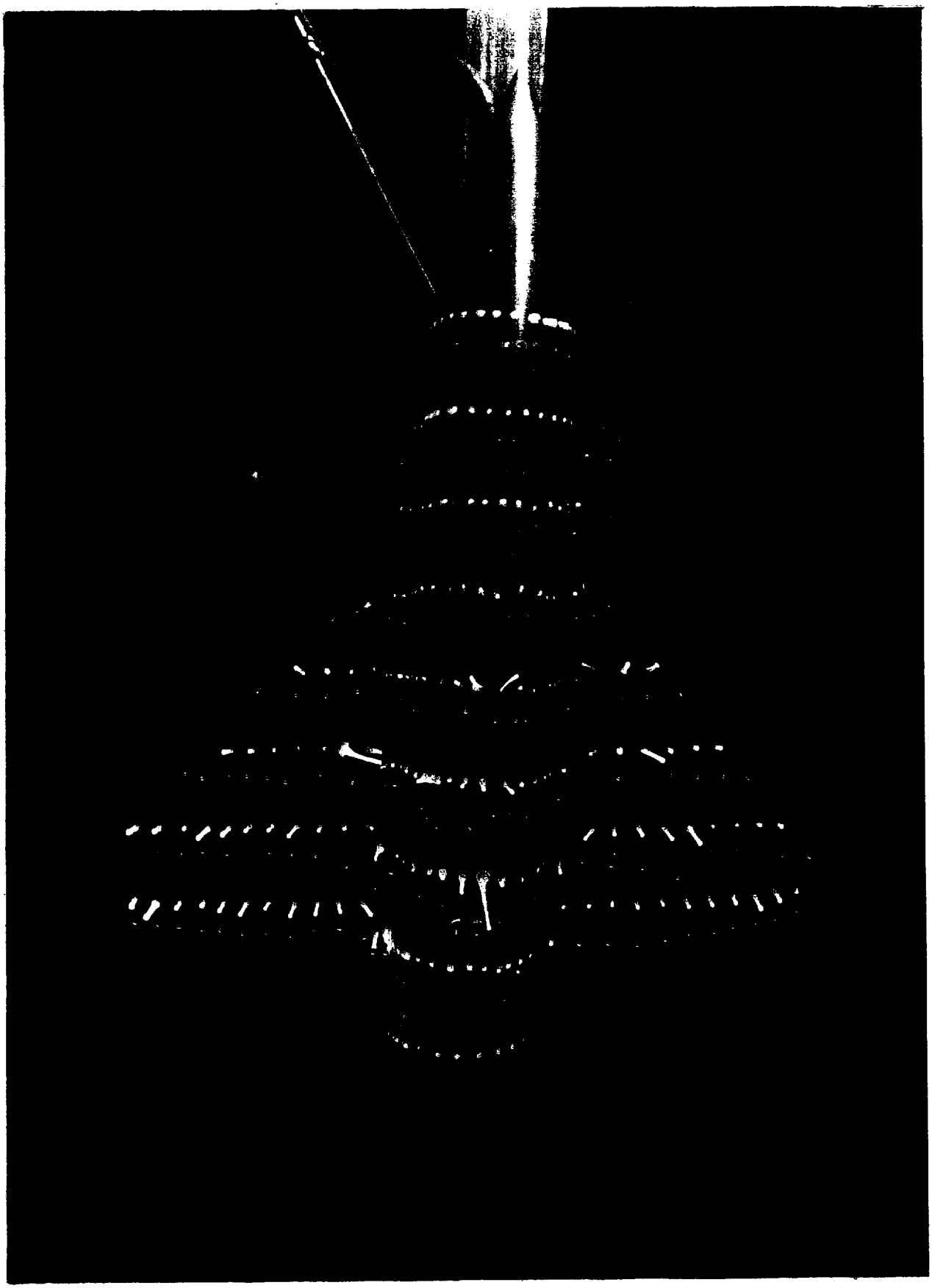

Figure 13. Flow pattern for the round body/high-wing combination at H = 10.44 in. (H/D_e = 6). (a) Lower surface view, NPR = 1.5.

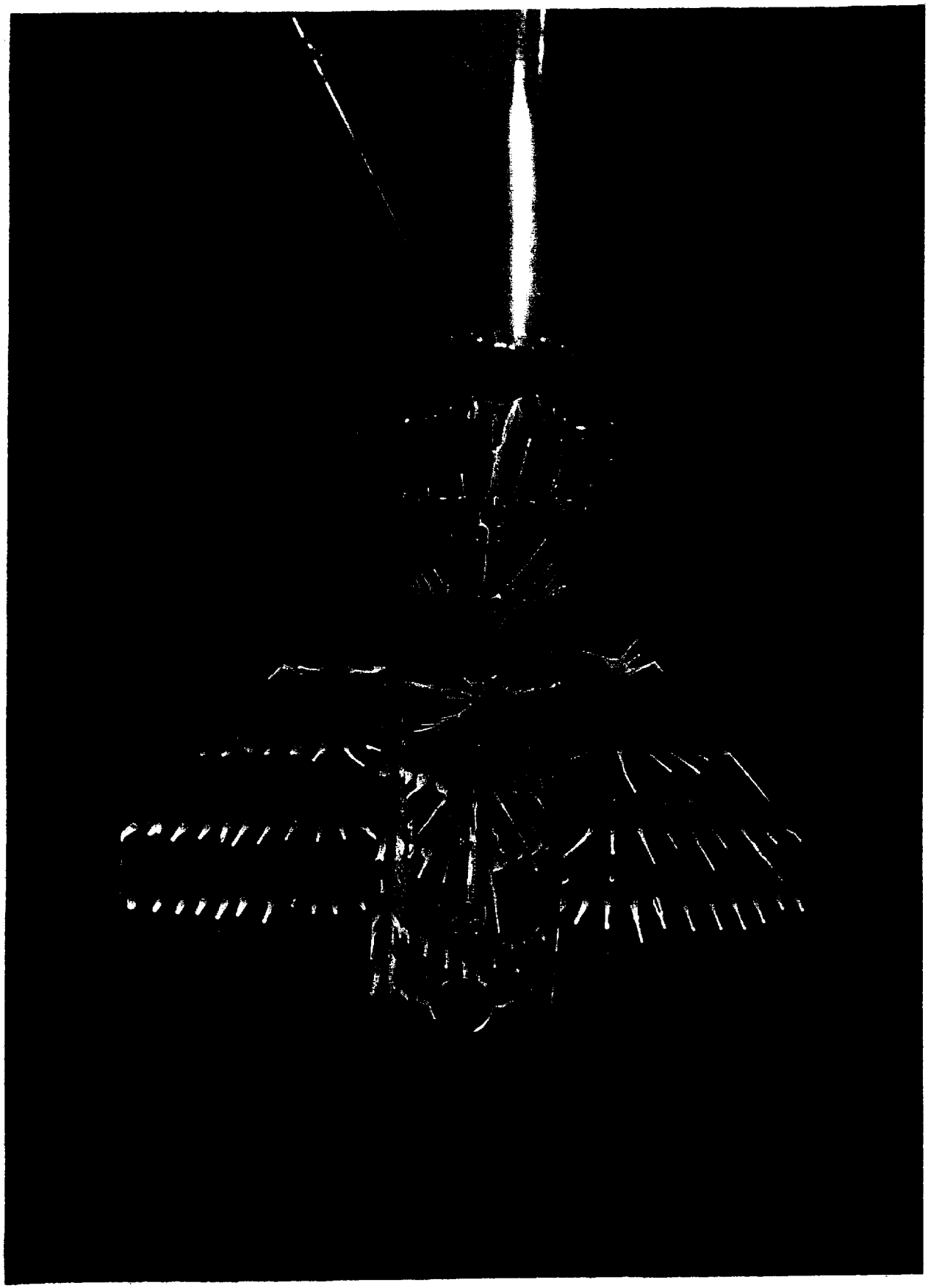

Figure 13. Continued. (b) Lower surface view, NPR = 3.0.

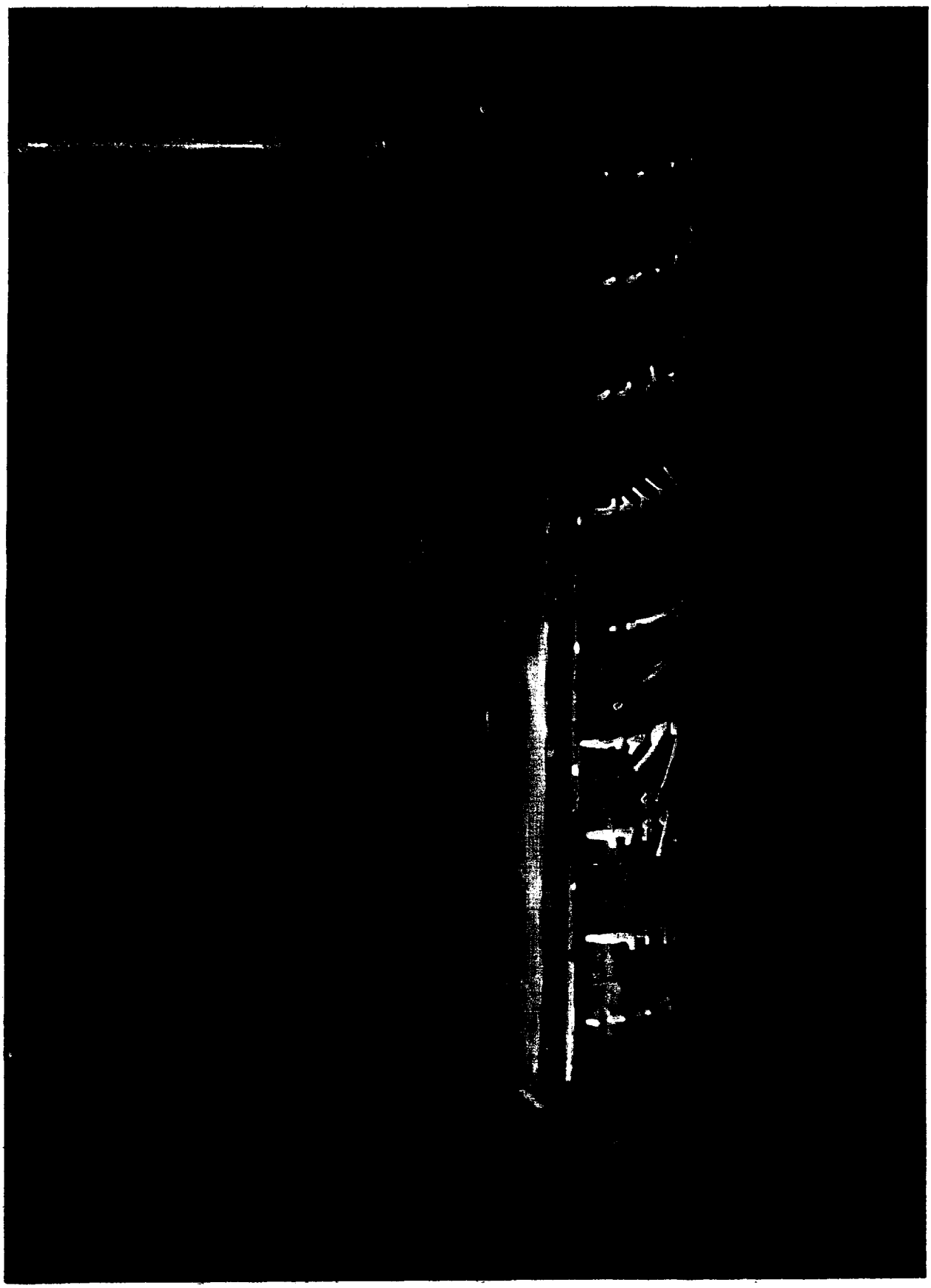

Figure 13. Continued. (c) Side surface view, NPR = 3.0.

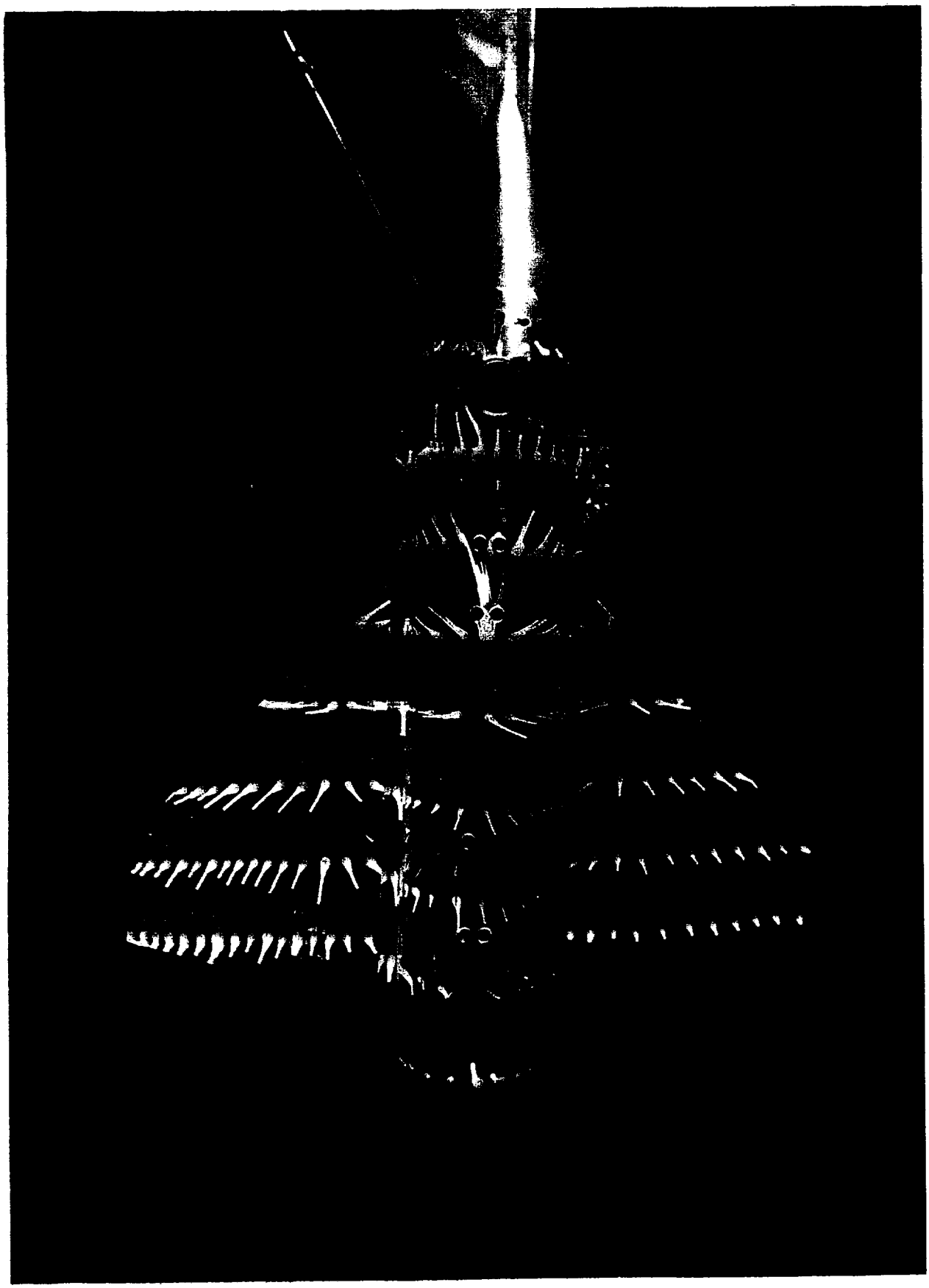

Figure 13. Continued. (d) Lower surface view, NPR = 4.5.

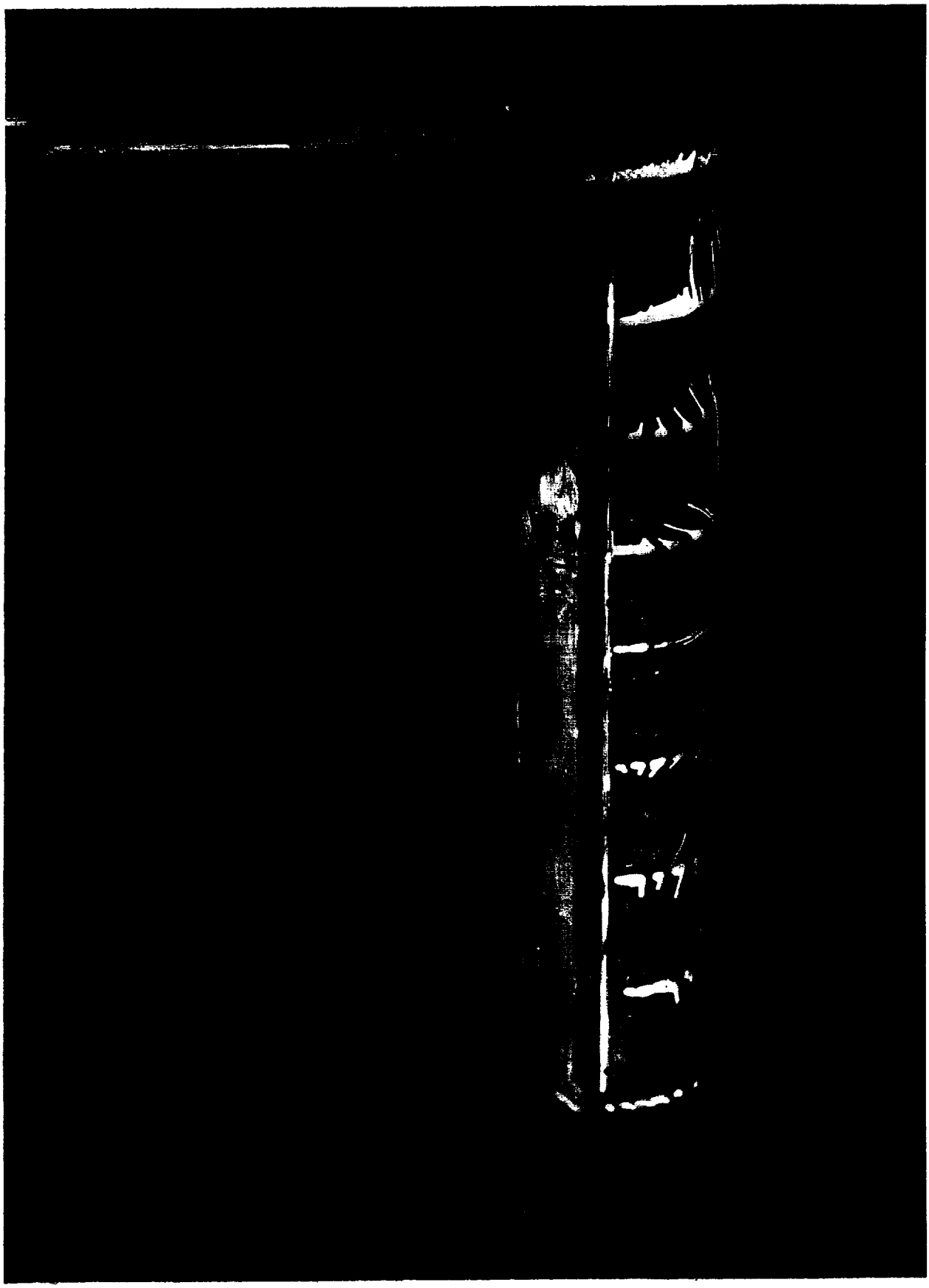

Figure 13. Continued. (e) Side view, NPR = 4.5.

Figure 13. Continued. (f) Lower surface view, NPR = 6.0.

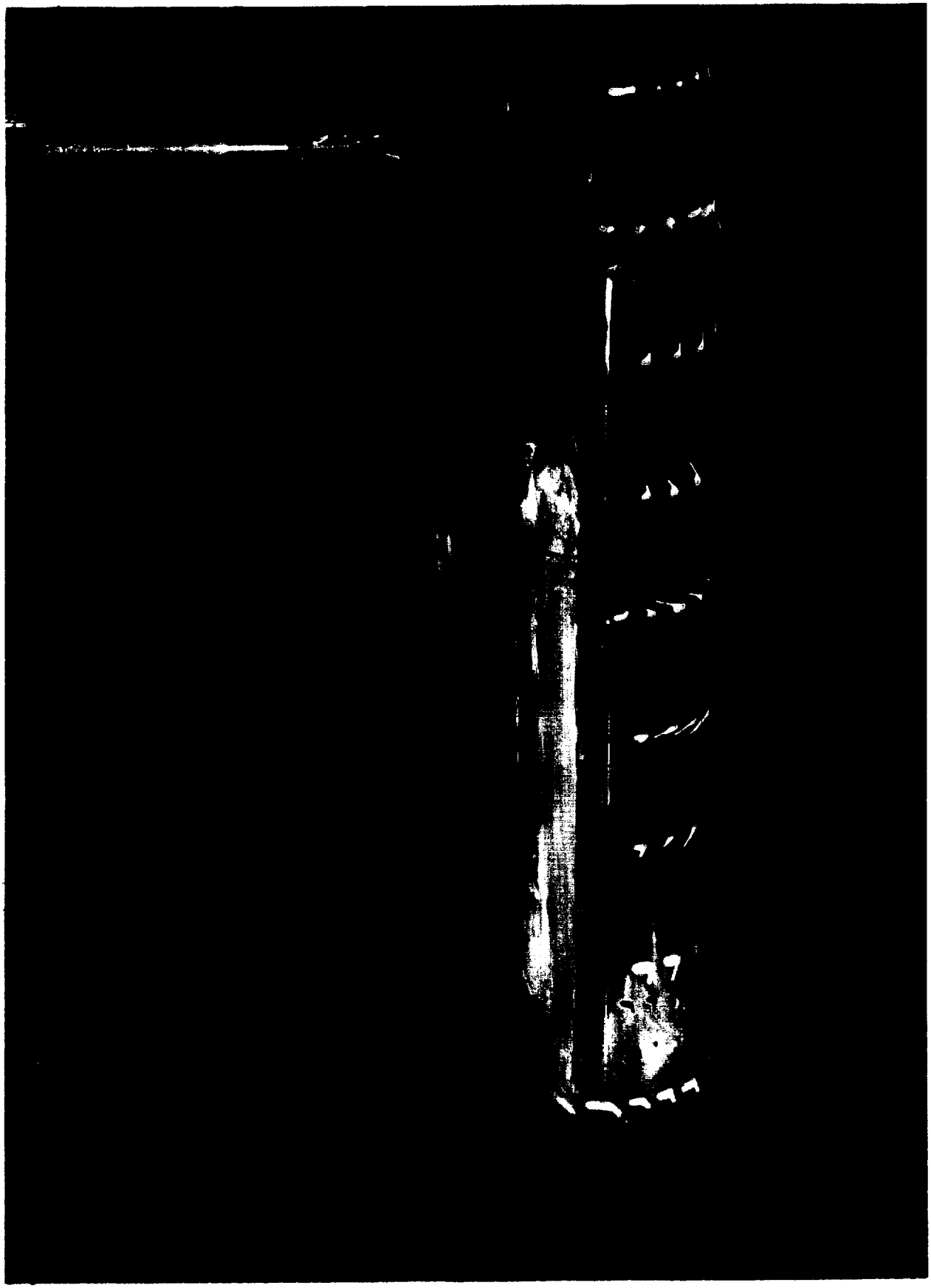

Figure 13. Concluded. (g) Side view, NPR = 6.0.

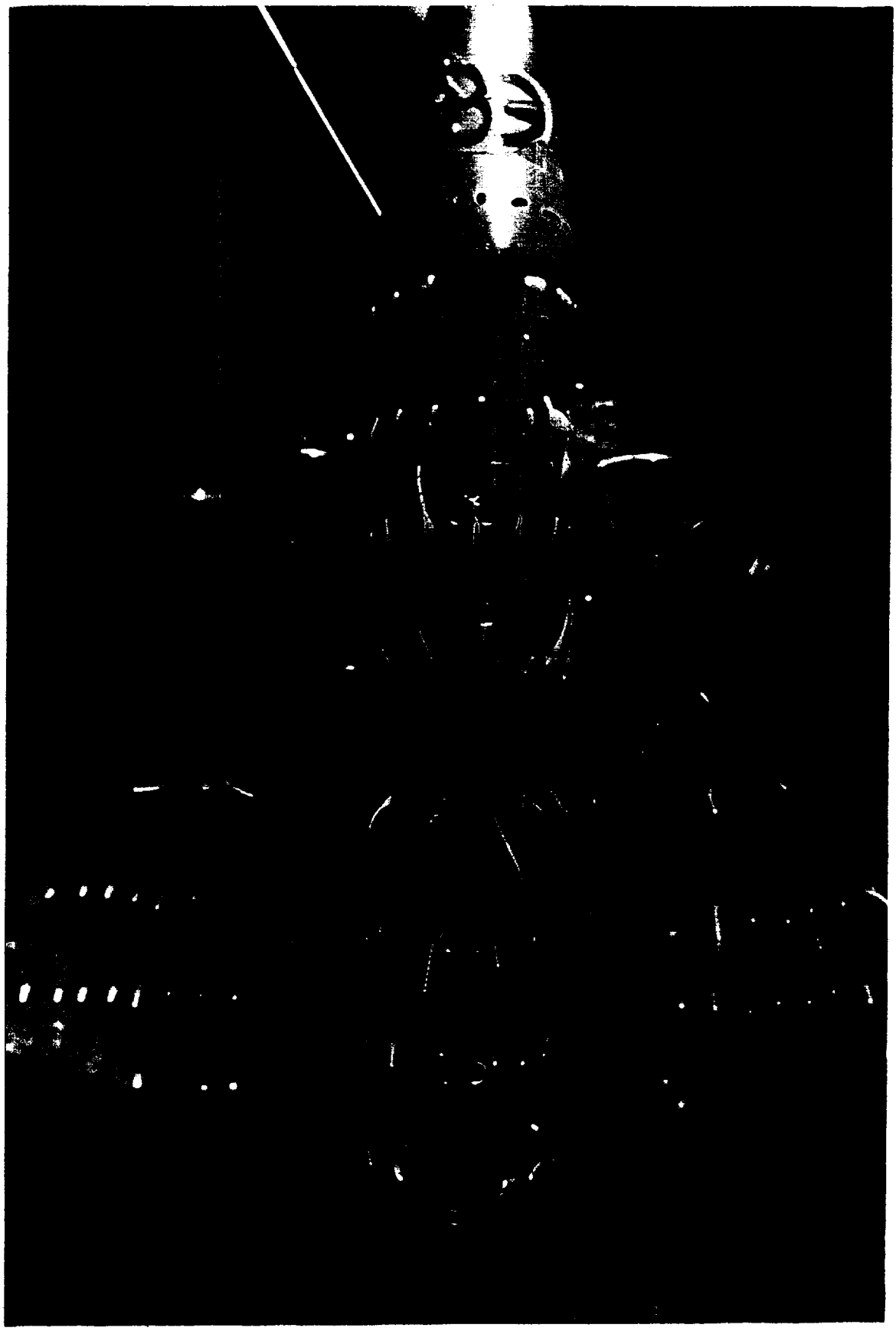

Figure 14. Undersurface flow pattern for the round body/high-wing combination with side inlets at $H = 3.48$ in. ($H/D_e = 2$). (a) Lower surface view, NPR = 1.5.

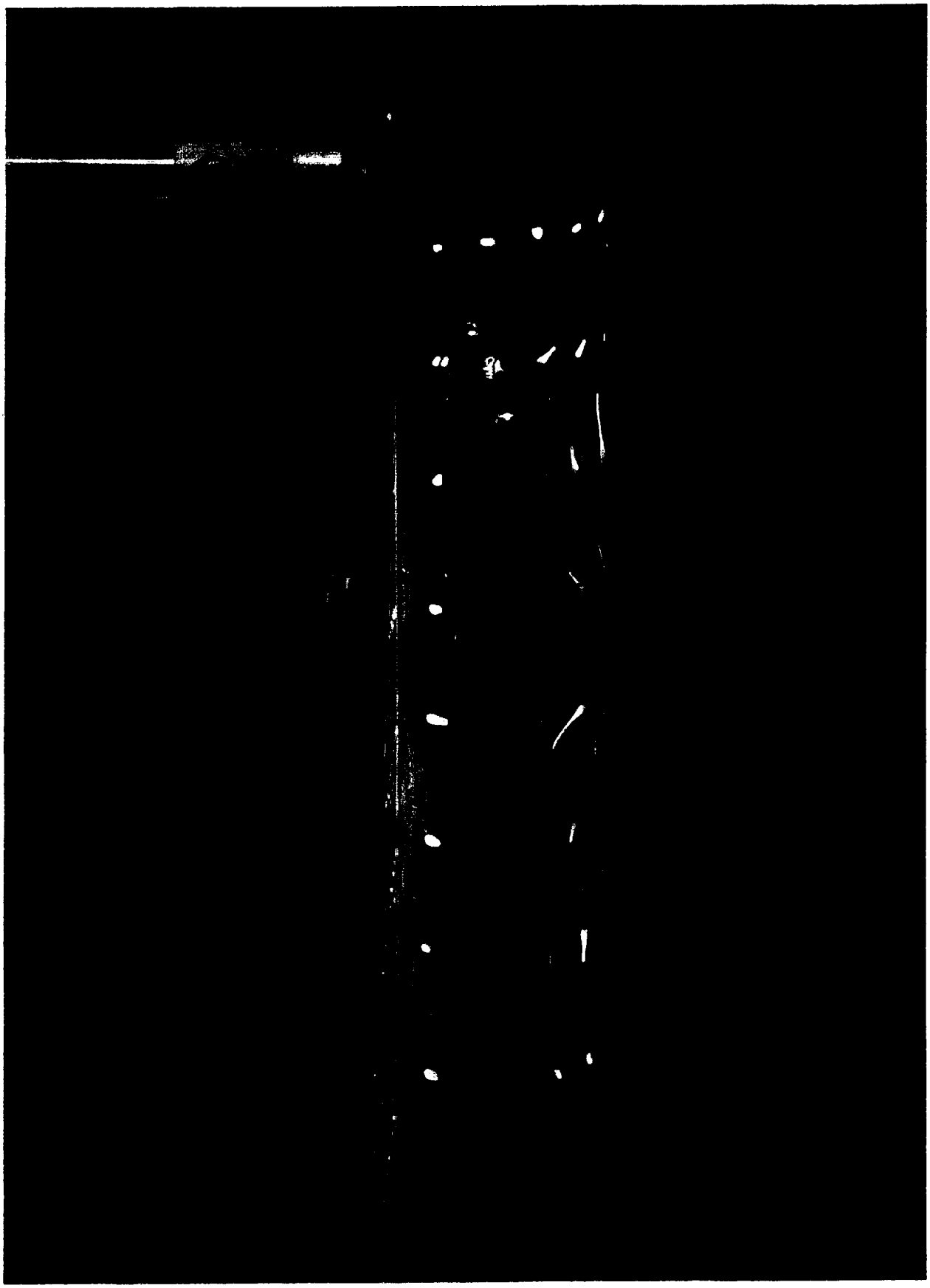

Figure 14. Continued. (b) Side view, NPR = 1.5.

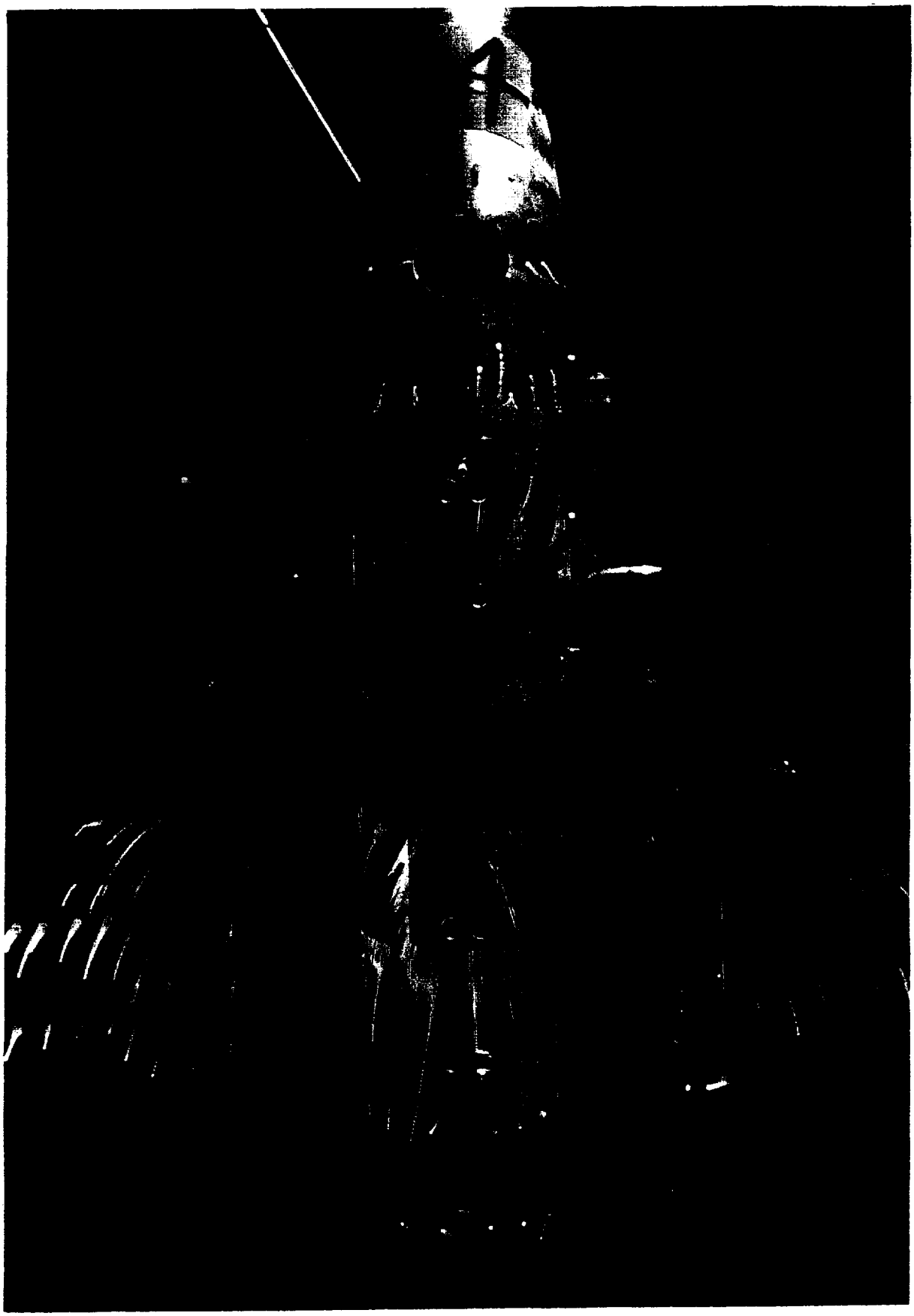

Figure 14. Continued. (c) Lower surface view, NPR = 3.0.

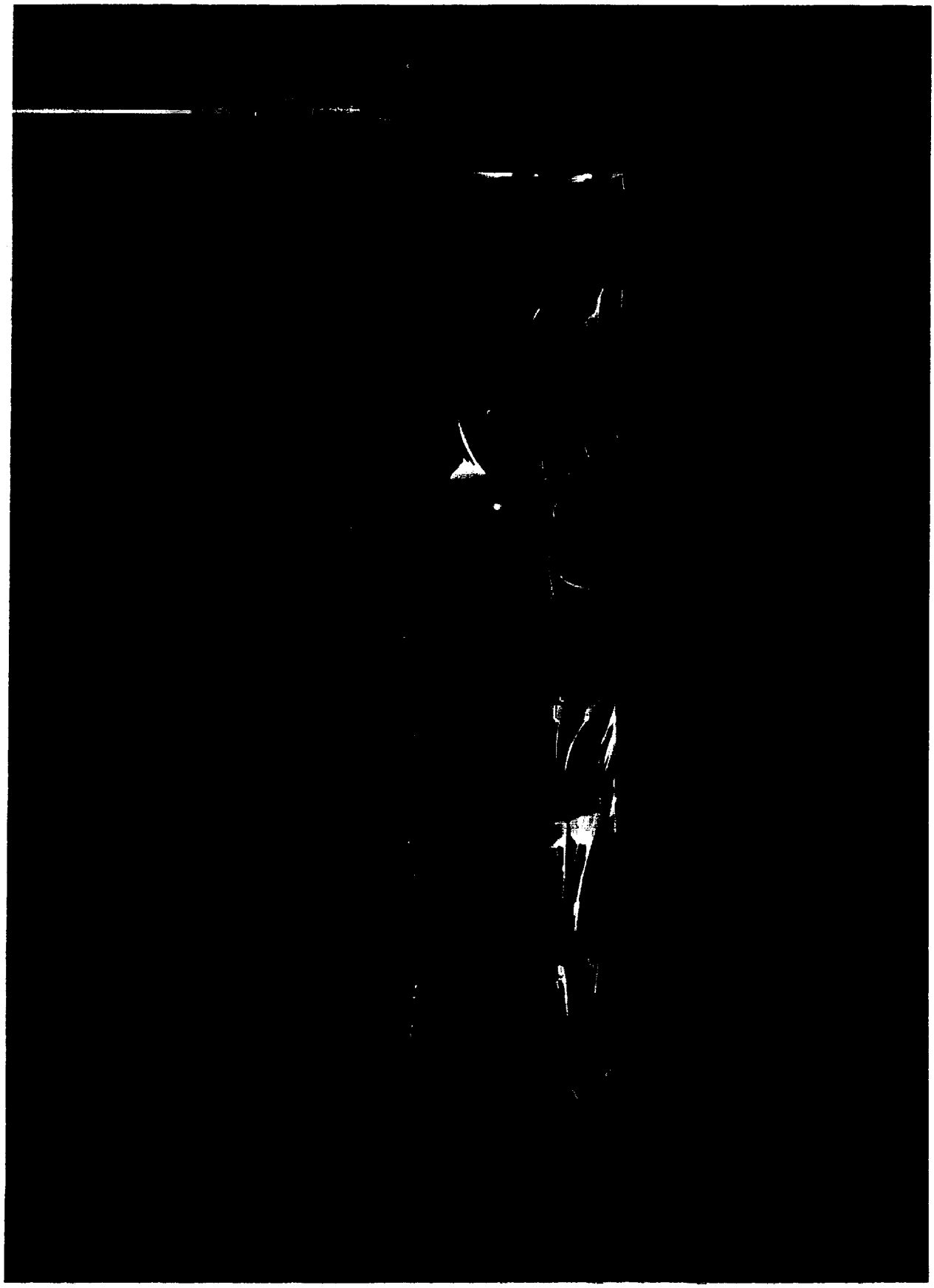

Figure 14. Continued. (d) Side view, NPR = 3.0.

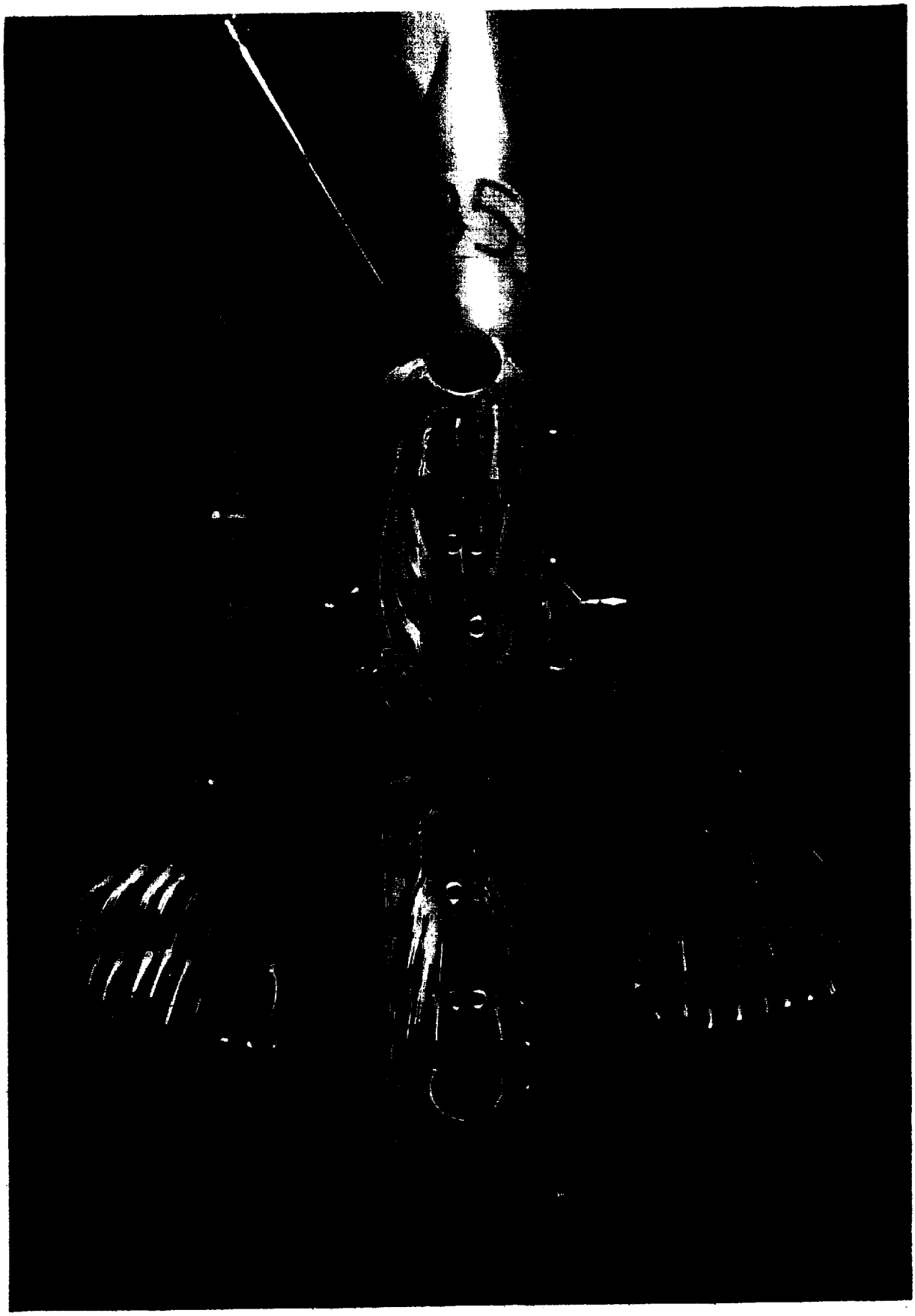

Figure 14. Continued. (e) Lower surface view, NPR = 4.5.

Figure 14. Continued. (f) Lower surface view, NPR = 6.0.

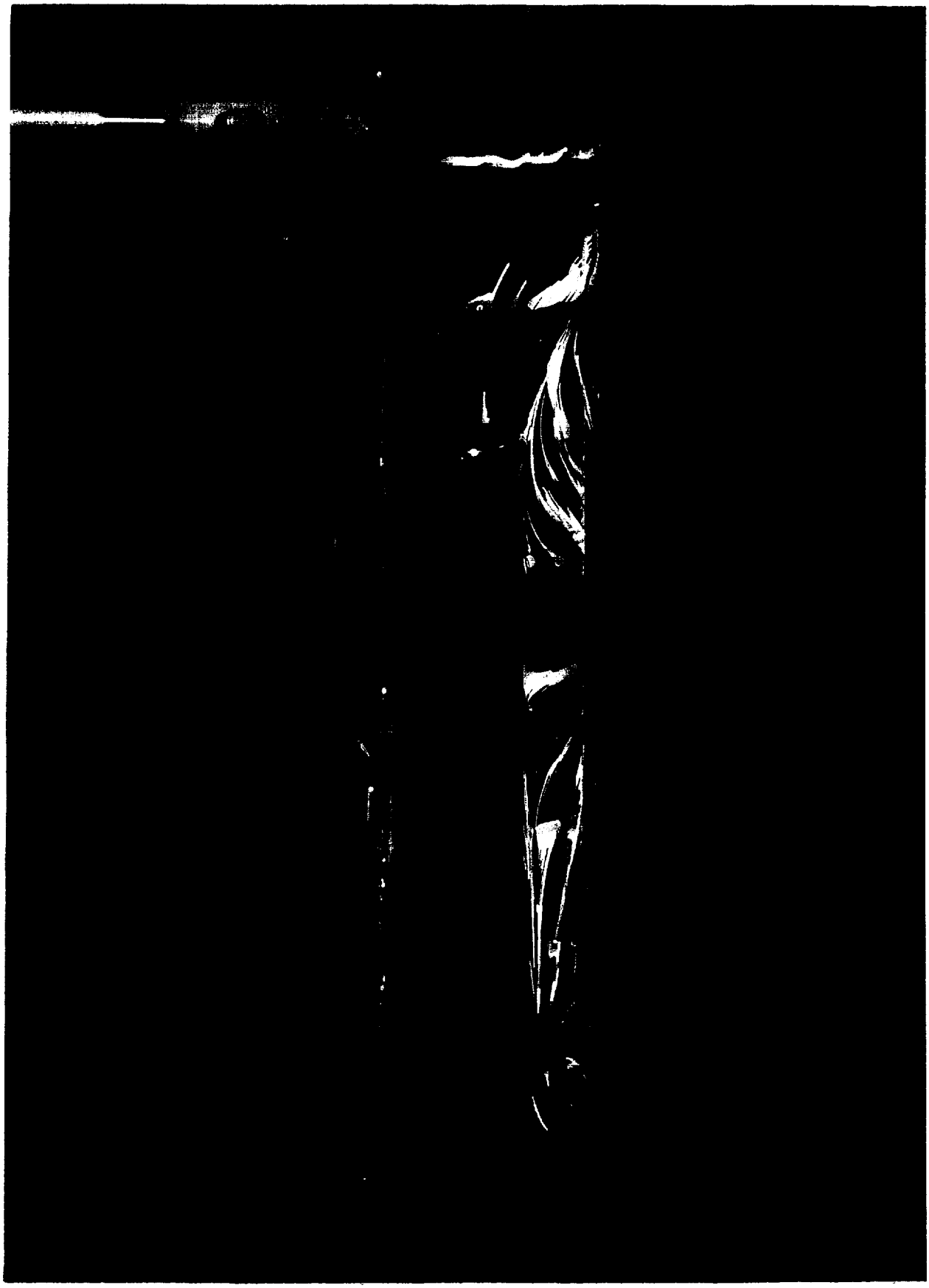

Figure 14. Concluded. (g) Side view, NPR = 6.0.

REPORT DOCUMENTATION PAGE

Form Approved
OMB No. 0704-0188

1. AGENCY USE ONLY *(Leave blank)*	2. REPORT DATE	3. REPORT TYPE AND DATES COVERED
	January 1995	Technical Memorandum

4. TITLE AND SUBTITLE

Flow Visualization Studies of VTOL Aircraft Models During Hover In Ground Effect

5. FUNDING NUMBERS

505-68-32

6. AUTHOR(S)

Nikos J. Mourtos,* Stephane Couillaud,* Dale Carter,* Craig Hange, Doug Wardwell, and Richard J. Margason

7. PERFORMING ORGANIZATION NAME(S) AND ADDRESS(ES)

Ames Research Center
Moffett Field, CA 94035-1000

8. PERFORMING ORGANIZATION REPORT NUMBER

A-95025

9. SPONSORING/MONITORING AGENCY NAME(S) AND ADDRESS(ES)

National Aeronautics and Space Administration
Washington, DC 20546-0001

10. SPONSORING/MONITORING AGENCY REPORT NUMBER

NASA TM-108860

11. SUPPLEMENTARY NOTES

Point of Contact: Richard J. Margason, Ames Research Center, MS 247-2, Moffett Field, CA 94035-1000; (415) 604-5033
*San Jose State University, San Jose, California.

12a. DISTRIBUTION/AVAILABILITY STATEMENT

Unclassified — Unlimited
Subject Category 02

12b. DISTRIBUTION CODE

13. ABSTRACT ***(Maximum 200 words)***

A flow visualization study of several configurations of a jet-powered vertical takeoff and landing (VTOL) aircraft model during hover in ground effect was conducted. A surface oil flow technique was used to observe the flow patterns on the lower surfaces of the model. There were significant configuration effects. Wing height with respect to fuselage, the presence of an engine inlet duct beside the fuselage, and nozzle pressure ratio are seen to have strong effects on the surface flow angles on the lower surface of the wing. This test was part of a program to improve the methods for predicting the hot gas ingestion (HGI) for jet-powered vertical/short takeoff and landing (V/STOL) aircraft. The tests were performed at the Jet Calibration and Hover Test (JCAHT) Facility at Ames Research Center.

14. SUBJECT TERMS

Hot gas ingestion, Flow visualization, Surface flow patterns, 2-jet configuration, Inlet flow

15. NUMBER OF PAGES

48

16. PRICE CODE

A03

17. SECURITY CLASSIFICATION OF REPORT	18. SECURITY CLASSIFICATION OF THIS PAGE	19. SECURITY CLASSIFICATION OF ABSTRACT	20. LIMITATION OF ABSTRACT
Unclassified	Unclassified		

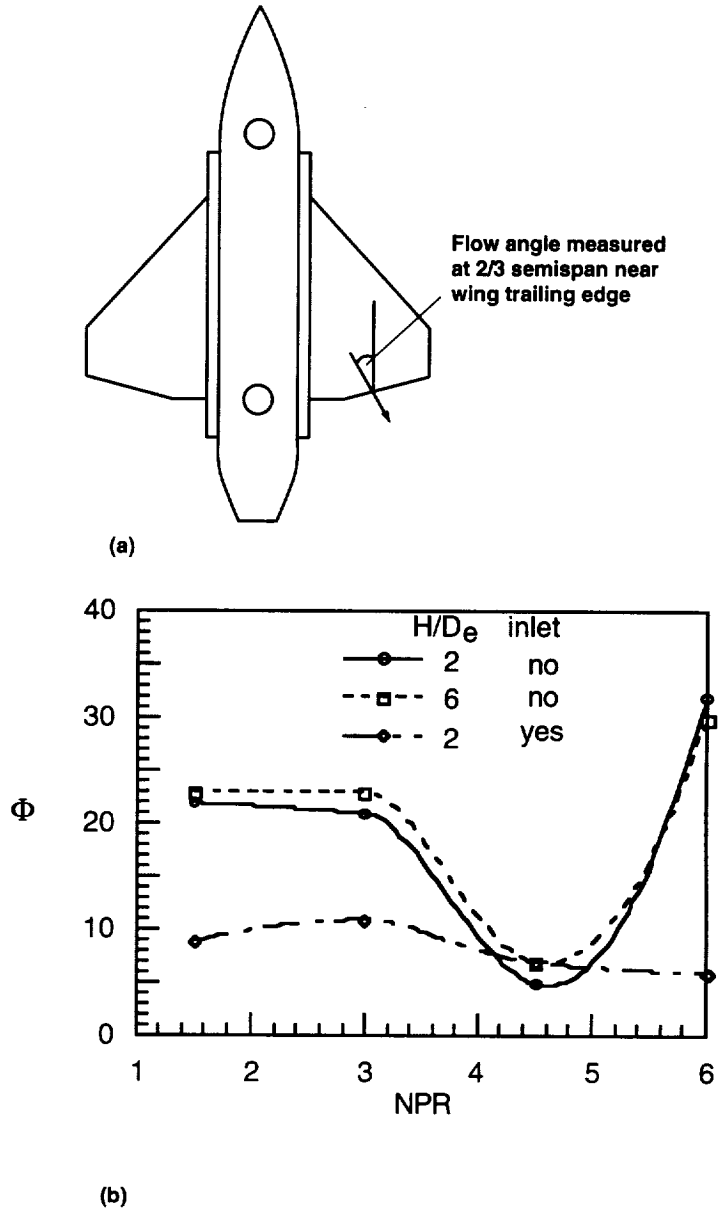

Figure 15. Effect of NPR on the location of the flow direction at the 2/3 semispan location of the wing trailing edge. (a) Sketch of wing-body and flow angle measurement Φ; (b) variation of flow angle with NPR.